Journal of Materials Chemistry B

PAPER

Check for updates

Double-crosslinkable poly(urethane)-based hydrogels relying on supramolecular interactions and light-initiated polymerization: promising tools for advanced applications in drug delivery†

Alessandro Torchio, [ID] ‡[a] Monica Boffito, [ID] ‡*[ab] Rossella Laurano,[a] Claudio Cassino, [ID] [c] Mario Lavella [ID] [d] and Gianluca Ciardelli [ID] *[ae]

Physical and chemical hydrogels are promising platforms for tissue engineering/regenerative medicine (TERM). In particular, physical hydrogels are suitable for use in the design of drug delivery systems owing to their reversibility and responsiveness to applied stimuli and external environment. Alternatively, the use of chemical hydrogels represents a better strategy to produce stable 3D constructs in the TERM field. In this work, these two strategies were combined to develop multi-functional formulations integrating both drug delivery potential and TERM approaches in a single device. Specifically, a novel photo-sensitive poly(ether urethane) (PEU) was developed to form supramolecular networks with α-cyclodextrins (α-CDs). The PEU was successfully synthesized using Poloxamer® 407, 1,6-diisocyanatohexane and 2-hydroxyethyl methacrylate, as assessed by infrared spectroscopy, size exclusion chromatography and proton nuclear magnetic resonance (^{1}H NMR) spectroscopy. Subsequently, PEU thermo-responsiveness was characterized through critical micelle temperature evaluation and dynamic light scattering analyses, which suggested the achievement of a good balance between molecular mass and overall hydrophobicity. Consequently, the formation of supramolecular domains with α-CDs was demonstrated through X-ray diffraction and ^{1}H NMR spectroscopy. Supramolecular hydrogels with remarkably fast gelation kinetics (*i.e.*, few minutes) were designed using a low PEU concentration (≤5% w/v). All formulations were found to be cytocompatible according to the ISO 10993-5 regulation. Notably, the hydrogels were observed to possess mechanical properties and self-healing ability, according to rheological tests, and their fast photo-crosslinking was evidenced (<60 s) by photo-rheology. A high curcumin payload (570 μg mL^{-1}) was encapsulated in the hydrogels, which was released with highly tunable and progressive kinetics in a physiological-simulated environment for up to 5 weeks. Finally, a preliminary evaluation of hydrogel extrudability was performed using an extrusion-based bioprinter, obtaining 3D-printed structures showing good morphological fidelity to the original design. Overall, the developed hydrogel platform showed promising properties for application in the emerging field of regenerative pharmacology as (i) easily injectable drug-loaded formulations suitable for post-application stabilization through light irradiation, and (ii) biomaterial inks for the fabrication of patient-specific drug-loaded patches.

[a] *Department of Mechanical and Aerospace Engineering, Politecnico di Torino, Corso Duca degli Abruzzi 24, 10129 Torino, Italy. E-mail: monica.boffito@polito.it, gianluca.ciardelli@polito.it*

[b] *Institute for Chemical-Physical Processes, National Research Council (CNR-IPCF), Via G. Moruzzi 1, 56124, Pisa, Italy*

[c] *Department of Science and Technological Innovation, Università del Piemonte Orientale "A. Avogadro", Viale Teresa Michel 11, 15121 Alessandria, Italy*

[d] *Department of Management, Information and Production Engineering, Università degli Studi di Bergamo, Viale G. Marconi, 5, 24044 Dalmine, BG, Italy*

[e] *Department of Life Sciences, University of Modena and Reggio Emilia, Via Campi 287, 41125 Modena, Italy*

† Electronic supplementary information (ESI) available: ATR-FTIR spectra of P407 and HHP407; CMT curves for HHP407 solutions; DLS volume patterns for HHP407 solutions; ^{1}H NMR spectra of CD-HHP407 complexes; appearance of samples after incubation with DMEM for 24 hours; cytocompatibility of CDs at different concentrations; appearance of Cur solution in EtOH *vs.* Cur dispersion within CD solution; strain sweep tests to study the self-healing properties of unloaded- and Cur-loaded formulations; rheological frequency sweep tests of Cur-loaded hydrogels; calibration curves used for Cur quantification. See DOI: https://doi.org/10.1039/d4tb00092g

‡ These authors have contributed equally to this work.

Introduction

Physical hydrogels are extremely interesting systems owing to their significant reversibility and processability. Indeed, the main advantage of physically crosslinked networks is represented by the possibility to easily perform injections and adapt them to external morphologies. Another advantage of these systems is their high tunability. Nonetheless, they are associated with some limitations. Most importantly, the development of stable and durable hydrogel networks based on physical interactions is challenging. Indeed, a relevant number of weak crosslinks is necessary to properly stabilize the polymeric network in an aqueous environment. Furthermore, the indispensable hydrophilicity that is characteristic of these systems induces the absorption of fluids from the external environment. This natural process can lead to mass exchange with the external environment, and complete dissolution of the system may occur within few days. Although this behavior is ideal for most drug delivery applications since several therapeutic drugs are characterized by high hydrophobicity and low bioavailability and hence need specific carriers for their delivery, it represents a strong limitation in the prolonged administration of therapies. This issue is well-known and has been widely discussed by various authors.[1,2]

Accordingly, a possible solution to overcome this drawback is the development of chemically crosslinked hydrogel networks. However, this strategy is generally associated with low responsiveness and limited handling.[3] Moreover, chemical additives are often necessary to carry out the crosslinking process, which may induce toxic effects.[4]

In this case, a relatively broader approach involves the integration of both the physical and chemical crosslinking methods in a single hydrogel formulation with the ultimate goal of combining the advantages of both strategies, while reducing the related deficiencies. In this regard, the appropriate selection of the chemical composition and the resulting physical properties are essential factors to successfully develop hybrid strategies based on both chemical and physical crosslinking. Indeed, the tuning of the physical interactions originating from the constituent polymeric units in combination with additional chemical crosslinking can result in highly stiff and stable hydrogels, as reported, for example, in the work by Li *et al.*, in which a hydrogel system characterized by an elastic modulus around 5 MPa and a strength equal to 2.5 MPa was described.[5] In detail, the authors discussed how hydrogel network organization and the nature of the occurring interactions account for the development of formulations with a remarkable mechanical response. In this work, they developed a hydrogel network stabilized through crystalline (physical) and covalent (chemical) domains using poly(vinyl alcohol) (PVA) to form crystallites and poly(acrylamide) (PAA) to generate chemical bonds. Consequently, they obtained a hydrogel system with mechanical properties very similar to that of natural tissues, such as cartilage and skin. In this case, chemical crosslinking was pursued through the overnight *in situ* polymerization of acrylamide in the presence of *N,N*′-methylenebisacrylamide

(MBAA) and tetramethyl-ethylenediamine (TEMED) at room temperature. This approach can be considered a "macromolecular" strategy, in which the organization of the resulting network is based on standard intermolecular interactions.

Nonetheless, a more sophisticated and versatile approach can also be pursued relying on supramolecular (SM) self-assembly. In this case, the initial processability of physical hydrogels is preserved due to the adaptivity of the SM networks and subsequent *in situ* stabilization can be performed through chemical crosslinking. Hence, highly organized SM networks can be *ad hoc* engineered to exhibit appropriate functionalities for further and fast chemical stabilization, which induces mechanical strengthening and improves their resistance to solubilization. In this regard, the chemical composition of all the components of the derived hydrogel systems is even more important in terms of tuning and engineering. An interesting example describing this approach can be found in the work conducted by Zhao and co-authors.[6] In this case, a modified di-acryloyl block co-polymer was synthesized using Pluronic® F68 (also commercially available as Poloxamer® 188, P188) and poly(ε-caprolactone) (PCL) with the aim to exploit its photo-sensitivity to ensure fast polymerization after complete self-assembly into poly(pseudo)rotaxanes (PPRs) with α-cyclo-dextrins (α-CDs).[7–12] The resulting hydrogel systems were characterized by notably high mechanical properties (*i.e.*, storage modulus (G') greater than 100 kPa) and good responsiveness in aqueous environments (*i.e.*, the equilibrium swelling ratio of the developed formulations was dependent on the molar feed ratio of α-CDs to the macromer). Another similar work was conducted by the same authors utilizing the same macromer in the presence of β-CDs, thus further proving the versatility of appropriately synthesized amphiphilic polymers in enabling the *ad hoc* engineering of hydrogels best matching the specific requisites of each envisaged application.[13] In contrast, Wei and co-workers developed an interesting system composed of star-shaped photo-curable macromers and α-CDs.[14] In detail, they synthesized a methacryloyl-terminated poly(L-lactide)-*b*-poly(ethylene glycol) (PLA-*b*-PEG) copolymer consisting in three or four arms and formulated SM hydrogels by adding α-CDs in aqueous solution. The presence of photocurable domains was demonstrated to improve mechanical strength and stability of the derived SM networks in an aqueous environment. Moreover, these systems showed a highly tunable responsiveness in aqueous environment, reaching a swelling ratio of up to 500% within 7 days of incubation in an aqueous medium. The same research group developed other similar systems based on the same strategy.[15,16]

In the last decade, although few research works focused on the specific design of photo-crosslinkable PPR-based networks, the general importance of developing shear-thinning and self-healing hydrogels retaining potential for secondary crosslinking has attracted continuously increasing interest. Indeed, the combined possibility to easily process a hydrogel matrix that is intrinsically self-sustaining, and then further stabilize it through fast photo-crosslinking also represents an extremely important feature for the development of bioinks and

8390 | *J. Mater. Chem. B*, 2024, **12**, 8389–8407

This journal is © The Royal Society of Chemistry 2024

biomaterial inks for extrusion-based 3D printing. The most recent and relevant strategies underpinning this idea have been reviewed and critically analyzed by many researchers.[17–19] Specifically, in these publications, the authors debated the key role played by mechanical features in the development of highly effective and functional hydrogel bioinks and biomaterial inks. In this regard, supramolecular-based matrices represent one of the most promising strategies to ensure self-healing and shear-thinning responses, which are elemental features for injection or printing of even cell-laden hydrogels.

Accordingly, based on the promising results reported in our previous publications,[20,21] this work was conceived with the aim of designing a new platform of double-crosslinkable hydrogels relying of physical SM interactions and chemical bonds resulting from light-initiated radical polymerization. Specifically, herein, novel SM and photo-curable systems based on a new synthesized poly(ether urethane) (PEU) were developed. In fact, *ad hoc* designed PEUs retain huge potential as materials for the fabrication of medical devices due to their LEGO-like chemical structure. This peculiarity has been widely exploited in previous studies aiming to properly fulfil various technical and clinical needs.[22–28] In detail, our previous findings indicated that Poloxamer® 407 (P407)-based PEUs are the best materials for the formation of PPR-based networks with α-CDs due to their balanced match among molecular mass, hydrophobicity and overall macromolecular functionality induced by chemical domains and structures. Based on these results, a new photo-sensitive PEU based on P407 and 1,6-hexamethylene diisocyanate (HDI) was synthesized by end-capping the pre-polymer chains produced at the end of the first step of the reaction through the addition of 2-hydroxyethyl methacrylate (HEMA). Consequently, a further improvement in the gelling ability of the resulting formulations was expected due to the significant reduction in polymers molar mass and concomitant preservation of the hydrophobic character derived from the partial polymerization reaction. The proposed approach has the advantage of combining both the potential to form physical hydrogels with α-CDs and the exposure of pendant photo-curable moieties in a single polymeric backbone. Subsequently, complete physico-chemical characterization of the synthesized PEU was performed through size exclusion chromatography (SEC) and attenuated total reflectance–Fourier transformed infrared (ATR-FTIR) spectroscopy, and proton nuclear magnetic resonance (^{1}H NMR) spectroscopy. The assessment of PEU thermo-responsiveness was conducted through dynamic light scattering (DLS) analyses and evaluation of the critical micelle temperature (CMT) of its aqueous solutions. Then, a new platform of photo-curable SM hydrogels was designed by mixing PEU and α-CD solutions and the most promising formulations were selected for rheological and photo-rheological characterization, as well as cytotoxicity evaluation according to the ISO 10993-5 regulation. Subsequently, curcumin was encapsulated within these novel PEU-based hydrogels as a notable example of highly hydrophobic (water solubility of approx. 3×10^{-8} M)[29] and environment-sensitive (poor chemical stability under physiological conditions) drugs.[30–32] The release profiles of curcumin from the physical and photo-cured hydrogels were obtained through incubation in an aqueous medium in highly destabilizing and physiological-like conditions (*i.e.*, in phosphate buffered saline solution at pH 7.4 and 37 °C). Finally, the suitability of the developed formulations for rapid prototyping purposes was preliminary evaluated using a commercial extrusion-based 3D-printing set-up. In summary, this work was conceived to prove the versatility of the PEU synthesis process as an effective tool to produce highly functional and tunable hydrogel systems for potential application as carriers of therapeutic agents in drug delivery and the emerging field of regenerative pharmacology.

Experimental

Materials

Poloxamer® 407 (P407, $\overline{M}_n$ 12 600 Da, 70% w/w poly(ethylene oxide)), 1,6-hexamethylene diisocyanate (HDI), 2-hydroxyethyl methacrylate (HEMA), dibutyltin dilaurate (DBTDL) and 3-(trimethylsilyl)propionic-2,2,3,3-d 4 acid sodium salt (TSP) were obtained from Merck/Sigma-Aldrich (Milan, Italy). α-CDs (herein, simply indicated with the acronym "CDs") and lithium phenyl-2,4,6-trimethylbenzoylphosphinate (LAP, a photo-initiator) were purchased from TCI Chemicals Europe (Zwijndrecht, Belgium). All solvents were purchased from Carlo Erba Reagents (Milan, Italy) in analytical grade and used as received unless otherwise stated. Before the synthesis, P407 was dried under mild vacuum (*ca.* 150 mbar) at 100 °C for 8 h, and then kept at 40 °C under vacuum until use. HEMA was dried and stored in a desiccator at low pressure (approx. 1–5 mbar) and room temperature, while 1,2-dichloroethane (DCE) was dehydrated over activated molecular sieves (3 Å, Sigma Aldrich, Milan, Italy) under an N$_2$ flow. HDI was distilled under reduced pressure to completely remove moisture and stabilizers.

Synthesis of the photo-sensitive poly(ether urethane)

The photo-sensitive PEU used in this work was synthesized in two steps according to the protocol reported in our previous works with slight modifications.[21,23,25] In detail, in the first step of the synthesis, a prepolymer was produced by reacting P407 (20% w/v) with HDI (2:1 molar ratio with respect to P407) for 2.5 h at 80 °C in anhydrous DCE under a nitrogen atmosphere. Differently, the second step of the reaction involved the end-capping of the isocyanate-terminated prepolymer chains through the addition of HEMA (3% w/v in anhydrous DCE, 2:1 molar ratio with respect to P407). The reaction was conducted for 3 h at room temperature under stirring and protected from any source of light to avoid the occurrence of side reactions. Then, the reaction was stopped through the addition of methanol to passivate any exposed and unreacted isocyanate groups. The solution containing the end-capped PEU was precipitated in petroleum ether (4:1 volume ratio with respect to total DCE volume) at room temperature under vigorous agitation and in the dark. The supernatant was separated from the precipitated PEU, which was kept under a fume hood

This journal is © The Royal Society of Chemistry 2024

J. Mater. Chem. B, 2024, **12**, 8389–8407 | **8391**

overnight to allow drying. Subsequently, the dried PEU was solubilized again in DCE at 20% w/v concentration and purified through precipitation in a mixture of diethyl ether and methanol (98 : 2 v/v, 5 : 1 volume ratio with respect to DCE volume) in the dark. The purified PEU was collected through centrifugation (Hettich, MIKRO 220R, Tuttlingen, Germany) at 0 °C and 6000 rpm for 20 min and dried under a fume hood overnight. The resulting dried polymer was collected and stored under vacuum at 3 °C in the dark until use. The obtained PEU was denoted as HHP407, where the first H refers to the chain extender (HEMA), the second H identifies the diisocyanate (HDI) and P407 indicates the macrodiol.

Physico-chemical characterization of HHP407

Attenuated Total Reflectance – Fourier Transform Infrared (ATR-FTIR) spectroscopy. The successful synthesis of HHP407 was demonstrated through ATR-FTIR spectroscopy, which was performed at room temperature on PEU powder utilizing a PerkinElmer (Waltham, MA, USA) Spectrum 100 Instrument equipped with an ATR accessory with a diamond crystal (UATR KRSS). Each spectrum was obtained from 16 scans (4 cm^{-1} resolution) in the wavenumber range of 4000 to 600 cm^{-1}. The data analysis was conducted using the PerkinElmer Spectrum software. As control sample, the spectrum of P407 was recorded using the same protocol.

Size Exclusion Chromatography (SEC). The molar mass distribution of HHP407 was characterized using an Agilent Technologies 1200 Series (California, USA) SEC equipped with a refractive index detector (RID) and two Waters Styragel columns (HR1 and HR4). N,N-Dimethylformamide (DMF, HPLC grade, Carlo Erba Reagents, Milan, Italy) containing LiBr at a concentration of 0.1% w/v was utilized as mobile phase at a flow rate of 0.4 mL min^{-1}. Subsequently, the registered RID and elution volume data were exported as .CSV files. The number average molar mass ($\overline{M_n}$), weight average molar mass ($\overline{M_w}$) and dispersity index ($D = \overline{M_w}/\overline{M_n}$) were calculated using Microsoft Excel (Office 365, Microsoft Corporation, USA) and a specific calibration curve obtained from poly(ethylene oxide) (PEO) standards with peak molecular weight (M_p) ranging from 982 to 205 500 Da. For sample preparation, 2 mg of PEU were dissolved in 1 mL of DMF with LiBr added and filtered using poly(tetrafluoroethylene) (PTFE) syringe filters (0.45 μm, LLG International, Meckenheim, Germany).

Proton Nuclear Magnetic Resonance (^{1}H NMR) spectroscopy. ^{1}H NMR characterization was performed using an AVANCE III Bruker spectrometer equipped with an 11.75 T superconducting magnet (500 MHz ^{1}H Larmor frequency) and a Bruker BVT-3000 unit for temperature control. NMR spectra were obtained at 300 K after 10 min equilibration at 25 °C. Each spectrum was obtained as the average of 12 scans, with a relaxation time of 10 s. A sealed capillary containing 1 mM TSP in deuterium oxide (D$_2$O) was inserted in the NMR tube and used as reference for zeroing the chemical shift scale. Samples for ^{1}H NMR spectroscopy were obtained by solubilizing HHP407 in D$_2$O (99.8%, Sigma Aldrich, Italy) at a concentration of

10 mg mL^{-1}. The MNova software (Mestrelab Research, S. L, Spain, https://www.mestrelab.com) was utilized for elaboration of the spectra.

Investigation of the thermo-responsiveness of HHP407 aqueous solutions

Critical micelle temperature (CMT) evaluation. The evaluation of CMT was carried out to investigate the temperature-dependent behavior of HHP407 aqueous solutions. 1,6-diphenyl-1,3,5-hexatriene (DPH, Sigma Aldrich, Milan, Italy) fluorescent dye (4 × 10^{-4} mol L^{-1} in methanol) was added to PEU solutions (1% w/v concentration) previously prepared in double demineralized water (ddH$_2$O) or phosphate buffered saline (PBS, pH 7.4, Sigma Aldrich, Milan, Italy) at a final concentration of 2 × 10^{-5} mol L^{-1}. Then, the self-assembly of micelles was studied using an UV-Visible spectrophotometer (PerkinElmer Lambda 25 UV/VIS spectrometer, Waltham, MA, USA) in the temperature range of 5 °C to 40 °C at a rate of 1 °C step^{-1} with an equilibration time of 5 min step^{-1}. As reported by Boffito et al.,[23] the absorbance peak at 356 nm, which is as an indicator of DPH solubilization within the micelle core, was represented as a function of temperature and the CMT value was obtained as the intercept between the linear regions before and after the inflection point, indicating the beginning of the micellization process.[33,34]

Dynamic Light Scattering (DLS). Dynamic Light Scattering analyses were performed to obtain additional information on the temperature-driven micellization of HHP407 polymeric chains in aqueous medium. In this case, HHP407 was solubilized at a concentration of 1% w/v in ddH$_2$O or PBS, and then analyzed using a Zetasizer Nano S90 (Malvern Instruments, Worcestershire, United Kingdom) instrument. Analyses were conducted at 25 °C and 37 °C upon sample thermal equilibration at each tested temperature for 5 min. The micelle hydrodynamic diameter was obtained as the average of three runs and the results are reported as mean ± standard deviation.

Preparation and characterization of HHP407- and CD-based SM complexes

Preparation of supramolecular complexes. The formation of inclusion complexes (ICs) between HHP407 and CDs was evaluated in ddH$_2$O by mixing their respective solutions. In detail, concentrated solutions of PEU were produced by solubilizing the total amount of PEU in ddH$_2$O at 3 °C overnight. Then, a clear solution of CDs with a concentration of 14% w/v was prepared, added to PEU solutions and the resulting samples were mixed using a vortex mixer (40 Hz, 20–30 s). The final samples were characterized by an HHP407 concentration of 1% w/v and the amount of CDs required to theoretically cover the 100% of the available ethylene oxide (EO) domains (i.e., CDs at 7.6% w/v concentration). The samples were incubated for 72 h at room temperature (i.e., 25 °C) to form ICs. The obtained crystalline matter based on PPR complexes was collected through centrifugation (Mikro 220R, Hettich, Germany) at 4500 rpm and 10 °C for 15 min. The samples containing SM structures were quenched and frozen using

8392 | J. Mater. Chem. B, 2024, **12**, 8389–8407

This journal is © The Royal Society of Chemistry 2024

liquid nitrogen and freeze dried (Martin Christ ALPHA 2–4 LSC, Germany) for 24 h. Hereafter, the obtained SM complexes are denoted as HHP407 1%–SM 100%, indicating that they were designed to theoretically reach complete coverage of the PEO domains through CDs. The recovery of the assembly procedure was estimated according to eqn (1).

$$\text{Recovery (\%)} = 100 - (w_{\text{initial}} - w_{\text{final}})/w_{\text{initial}} \times 100 \quad (1)$$

where w_{initial} is the initial dried mass of HHP407 and CDs mixed to produce the inclusion complexes and w_{final} is the dried mass of the crystalline matter recovered through centrifugation.

^{1}H NMR spectroscopy. ^{1}H NMR analyses were performed according to the previously described protocol. The SM specimen for ^{1}H NMR spectroscopy was obtained through solubilization of HHP407 1%–SM 100% in D_2O at a concentration of 5 mg mL^{-1}. The spectra of the control samples based on CDs and HHP407 were also recorded. The MNova software (Mestrelab Research, S. L, Spain, **https://www.mestrelab.com**) was utilized for elaboration of the spectra.

X-ray powder diffraction (XRD) analysis. X-ray powder diffraction (XRD) analysis. The XRD patterns of HHP407 1%–SM 100% were obtained using an X-ray diffractometer D5005 assembled with a Bragg–Brentano geometry and vertical goniometer theta/theta (the specimen holder was fixed, while the tube and detector were rotated). The instrument was also equipped with an Ni-filtered Cu Kα (1.542 Å) radiation source set at 40 kV and 40 mA. The tests were performed in step scan mode in the 2θ range of 5° to 30° at an increment rate of 0.1° step^{-1} and scan speed of 10 s step^{-1}. As control sample, HHP407 was also analyzed using the same protocol.

Preparation and characterization of HHP407- and CD-based SM hydrogels

Preparation of SM hydrogels. SM hydrogels were produced in Bijou sample containers (17 mm inner diameter, 7 mL volume capacity, Carlo Erba Reagents, Milan, Italy) using PBS (pH 7.4) with LAP added at 0.05% w/v concentration as solvent (PBS/LAP). Firstly, HHP407 was solubilized in the required amount of PBS/LAP overnight at 3 °C. Then, a clear solution of CDs in PBS/LAP was prepared at 14% w/v and added to the HHP407 solutions, thus obtaining gelling systems containing HHP407 at concentration in the range of 1% to 5% w/v and CDs in the concentration range of 7–10% w/v. The obtained mixtures were homogenized using a vortex mixer (40 Hz, 30 s), while gelation was carried out at room temperature (25 °C). The samples were protected from any source of light during their preparation and characterization to avoid undesirable photopolymerization. The HHP407-based samples were denoted as HHP407 X%–CD Y%, where X and Y indicate the concentration of HHP407 and CD (% w/v), respectively.

Qualitative evaluation of gelation time and phase-separation under isothermal conditions. The gelation kinetics of the SM hydrogels was qualitatively investigated through visual inspection at room temperature (25 °C). In detail, at predefined time steps (*i.e.*, every 1 and 5 min up to 1 h observation, and then every 10 min), the samples (1 mL prepared in Bijou sample containers) were inverted and their flow along the walls of the container was assessed. The "gel" state was characterized by a "no-flow" condition after 30 s of vial inversion. Once the gelation process was completed, the samples were maintained at the gelling temperature (25 °C) and visually evaluated every day up to 7 days to assess the occurrence of phase-separation phenomena.

Rheological characterization. Rheological characterization of HHP407-based SM gels was carried out using a stress-controlled rheometer (MCR302, Anton Paar GmbH, Graz, Austria) equipped with a Peltier system for temperature control and a 25 mm parallel plate configuration. The hydrogels were injected through a 5 mL syringe (2 mm tip, *ca.* 0.4 mL) on the lower plate of the rheometer previously equilibrated at 25 °C. The normal force was imposed at 0 N and the thickness of the sample was set at 0.6 mm for all characterizations. Strain sweep tests were carried out at 37 °C and 1 rad s^{-1} angular frequency by sweeping strain values from 0.01 to 500%. The samples that were firstly evaluated through strain sweep test were analyzed again after 15 min of recovery under quiescent state and isothermal conditions (37 °C) to characterize the hydrogel capability to self-heal after a relevant strain was applied (*i.e.*, 500%). Frequency sweep tests were performed within the linear viscoelastic region (strain at 0.1%) at 25 °C, 30 °C and 37 °C and angular frequency in the range of 0.1 to 100 rad s^{-1}.

Self-healing tests were also executed to evaluate the physical reversibility of the hydrogels when a cyclic strain was applied over time at 37 °C, according to the protocol described by Wu and co-workers with few modifications.[35] In detail, a constant strain (0.1%, 1 Hz, recovery phase) was initially applied to the SM hydrogels for 120 s; subsequently, complete rupture of the hydrogel network was caused by application of a remarkably higher deformation (100%, 1 Hz, rupture phase) for 60 s. This cyclic strain was applied on each hydrogel system trice, and finally the starting strain (0.1%, 1 Hz, recovery phase) was again applied to estimate the residual mechanical properties of each formulation.

Moreover, due to the photo-responsive nature of HHP407, a photo-rheological characterization was also performed on the same samples. In detail, the storage and loss modulus (G' and G'', respectively) trends of the SM hydrogels was registered as a function of time in oscillation (1 Hz, 0.1% strain, 0 N normal force) for 1 min before UV irradiation. Then, UV light exposure was applied for 1 min at 365 nm and 10 mW cm^{-2} and the parameters were registered for additional 2 min to assess the overall stability of the photo-crosslinked networks.

Biological characterization of the hydrogels. To assess the biological compatibility of the designed hydrogels, cell viability and cytotoxicity were both qualitatively and quantitatively evaluated on hydrogel extracts through Live/Dead staining (Invitrogen) and a multiplex assay, respectively. Moreover, the contribution of released CDs on cell metabolic activity was studied by setting up a dose–response test in the concentration range of 0–10 mg mL^{-1}. For these experiments, NIH-3T3 murine fibroblasts (ATCC® CRL-1658) were regularly cultured

This journal is © The Royal Society of Chemistry 2024

J. Mater. Chem. B, 2024, **12**, 8389–8407 | **8393**

Table 1 Formulations tested for their biological compatibility

Sample acronym	Solvent	Physical crosslinking	Chemical crosslinking[a]
HHP407 X%–CD Y% w/o LAP	PBS	X	
HHP407 X%–CD Y%	PBS/LAP	X	
HHP407 X%–CD Y% UV	PBS/LAP	X	X

[a] Through UV light exposure (365 nm, 10 mW cm^{-2}) for 1 min.

in complete medium (*i.e.*, Dulbecco's modified Eagle's medium (DMEM, ATCC$^{®}$) added with MycoZap PLUS (Lonza) antibiotic and 10% v/v Bovine Calf Serum (BCS, ATCC$^{®}$)) and maintained in a humidified environment at 37 °C, 5% CO$_2$. Before each experiment, the absence of mycoplasma contamination was assessed in the cell supernatant using the MycoAlert Plus Mycoplasma Detection Kit (Lonza) according to the supplier's instructions.

Preparation of hydrogel extracts and cyclodextrin solutions. Samples for cytotoxicity tests were prepared by weighing 250 mg of self-assembling HHP407-based hydrogels in Bijou sample containers. Three different conditions were tested to isolate the contribution of the main features of the hydrogels (*i.e.*, solvent composition and strategy for hydrogel crosslinking), as summarized in Table 1. The samples were acclimatized at 37 °C for 15 min, 2.5 mL (*i.e.*, 1 mL every 100 mg of hydrogel) of complete medium (37 °C) were gently added and the systems were incubated for 24 h at 37 °C. Then, the eluates were withdrawn and collected for the evaluation of cell cytotoxicity and viability. Extract sterility was ensured through filtration with 0.22 μm poly(ether sulfone) filters (Carlo Erba Reagents, Milan, Italy).

Evaluation of cell cytotoxicity and cell viability. Before cell seeding, 96-well plates were treated to improve cell adhesion. Specifically, gelatin type A (Sigma Aldrich/Merck, Milan, Italy) was first dissolved at a concentration of 1 mg mL^{-1} in sterile ddH$_2$O; then, the solution was filtered through 0.22 μm poly(ether sulfone) filters (Carlo Erba Reagents, Milan, Italy), and lastly, it was added to a well plate at 50 μL well^{-1}. Subsequently, the plates were incubated at 37 °C for 30 min, UV-sterilized, and finally, they were kept in a sterile cabinet overnight to allow complete water evaporation. Afterwards, NIH-3T3 murine fibroblasts were first collected through trypsinization, re-suspended in complete medium and seeded at 10 000 cells well^{-1}, as recently reported by Laurano *et al.*[36] Then, the plates were incubated under normal culture conditions for 24 h to allow adherence. Subsequently, the medium was removed and replaced with 100 μL of hydrogel extract or CD solution and incubated for 24 h. Cell viability/cytotoxicity was first qualitatively assessed through the Live/Dead assay performed following the procedure suggested by the supplier. Briefly, the supernatant was removed and the cells were washed with Dulbecco's Phosphate-Buffered Saline (DPBS). Subsequently, 100 μL of Live/Dead working solution (*i.e.*, 2 μM Calcein AM and 4 μM ethidium homodimer-1 in DPBS) were added to each well and the plate was incubated for 20 min at 37 °C. Lastly, live (green) and dead (red) cells were imaged

under a fluorescence microscope (Leica DM IL LED Fluo, Leica Mycrosystems, Varese, Italy). Cell cytotoxicity was quantitatively investigated by measuring the amount of lactate dehydrogenase released in the medium through the CytoTox-ONE™ homogeneous membrane integrity assay (Promega) according to the manufacturer's instructions. Briefly, the 96-well plate was first equilibrated at room temperature for 20 min, and then 100 μL of CytoTox-ONE reagent were added to each well. After 10 min of reaction, 50 μL of stop solution were added to each well, and lastly the fluorescence was quantified through a multimode plate reader (VICTOR X3, PerkinElmer) at Ex/Em 535/590 nm. Cell viability was quantitatively evaluated by measuring the cell metabolic activity through the CellTiter-Blue$^{®}$ cell viability assay (Promega) following the protocol provided by the manufacturer. Briefly, 20 μL of CellTiter-Blue$^{®}$ solution were added to each well and the 96-well plate incubated at 37 °C, 5% CO$_2$ for 3 h. Then, the fluorescence was measured through a multimode plate reader (VICTOR X3, PerkinElmer) at Ex/Em 535/590.

For all the experiments, cells cultured in complete medium and cells treated with a lysing solution were used as the negative and positive controls, respectively. Cytotoxicity and cell viability percentages were calculated with respect to the positive and negative control, respectively. Tests were performed in triplicate and results reported as the average value ± standard deviation.

Curcumin encapsulation within SM gels, characterization and release studies. A curcumin (Cur) suspension with a concentration of 1 mg mL^{-1} was prepared in a CD solution at 14% w/v in PBS/LAP. Ultrasonication (52 W, 20 kHz, Vibracell VCX130, Sonics, USA) was applied for 3 min using a probe and a water-ice bath to avoid evaporation phenomena. The stability of the obtained suspension was evaluated by visual inspection at room temperature (25 °C) to define the temporal window for practical use. Then, this suspension was added to HHP407-based solutions in PBS/LAP, thus obtaining SM hydrogels at specific HHP407, CD and Cur contents. Incubation at 25 °C was carried overnight out to ensure complete sample gelation.

The entire set of rheological and photo-rheological characterizations previously described was also conducted on Cur-loaded SM-based hydrogels to evaluate the effects of drug loading on the development of SM networks and UV light responsiveness.

SM hydrogels (0.5 mL) for release studies of Cur were prepared in glass vials (10 mm inner diameter, 4 mL volume capacity, Sigma Aldrich, Milan, Italy) and denoted as HHP407 X%–CD Y% Cur, where X and Y indicate the PEU and CD concentrations (% w/v), respectively. For all the selected formulations, two sets of 5 samples each were prepared to evaluate the behavior of the purely physical hydrogel networks and the additional contribution of photo-crosslinking. Upon UV light exposure (1 min at 365 nm and 10 mW cm^{-2}), the samples were identified with the acronym HHP407 X%–CD Y% Cur UV. Release studies were conducted on SM hydrogels at 37 °C after acclimatization for 15 min. Then, 1 mL of PBS (37 °C) was

8394 | *J. Mater. Chem. B*, 2024, **12**, 8389–8407

This journal is © The Royal Society of Chemistry 2024

gently added on top of each hydrogel sample. At precise time steps (2, 4, 6, 24 h and 3, 4, 7, 14, 21, 28 and 35 days), eluates were withdrawn and completely refreshed with PBS. Cur quantification was performed using a UV/Vis spectrometer (Perkin-Elmer Lambda 25 UV/VIS spectrometer, Waltham, MA, USA) by evaluating the absorbance peak at around 430 nm. Reference curves were obtained by specific standard solutions produced through hydrogel dissolution and subsequent dilution (Cur concentration range of 1 to 20 μg mL^{-1}).

Extrusion-based 3D printing of SM hydrogels. A preliminary evaluation of the extrudability of the HHP407-based hydrogels was performed utilizing a Cellink Inkredible+ bioprinter (Cellink, USA). The printed CAD design was characterized by a square grid (15 × 15 mm) based on two layers (0.45 mm filament diameter and 0.35 mm filament gap). The top view of the resulting geometry is reported in Fig. 1. The geometry was obtained utilizing the Solidworks 2019 CAD software (Dassault Systèmes SolidWorks Corporation), while Repetier Host v2.1.6 (Hot-World GmbH & Co. KG) was utilized for g-code file generation and optimization. The preparation of the hydrogel was conducted as reported above in the specific section with slight modifications. In detail, solutions composed of HHP407, CDs and Cur were transferred immediately after mixing (*i.e.*, during gelation) into syringes appositely supplied for the 3D-printer. After overnight incubation at room temperature (*i.e.*, 25 °C), the resulting hydrogel networks were kept at 37 °C and their extrudability was tested with three different syringe tips (200, 250 and 450 μm diameter). Constructs were printed into Petri supports (poly(styrene), 5 cm diameter, Carlo Erba Reagents, Milan, Italy) and analyzed through optical microscopy (Leica DM IL LED, Leica Microsystems, Milan, Italy). Geometrical parameters were estimated using the ImageJ software (https://imagej.nih.gov/ij/index.html). Photo-induced crosslinking was performed after the printing procedure utilizing a UV light source at 365 nm (10 mW cm^{-2}). Qualitative evaluation of the stability of 3D-printed structures was carried out through incubation in contact with PBS (pH 7.4, 5 mL) at room temperature (*i.e.*, 25 °C). As a proof of concept of the possibility to use the developed hydrogel formulations as

constituents of multi-layered self-standing structures, 25-layer cylinder constructs with a 0/90° pattern were also fabricated (300 μm layer thickness). The hydrogel formulation was prepared as reported above and 3D printed according to the parameters identified through the previously described preliminary extrusion tests. Photo-crosslinking (365 nm, 10 mW cm^{-2}, 30 s per layer) was performed layer-by-layer with the aim of providing the structures with a homogeneous cross-linking density along the Z-axis.

Statistical analysis

Statistical analysis was conducted using GraphPad Prism 8 for Windows 10 (GraphPad Software, La Jolla, CA, USA; https://www.graphpad.com). Two-way ANOVA analysis coupled with the Bonferroni multiple comparison test was performed to compare results, assessing the statistical significance according to Boffito *et al.*[23] The significance level was assigned depending on the *p*-values, as follows: $p < 0.0001$ extremely significant (****), $0.0001 < p < 0.001$ extremely significant (***), $0.001 < p < 0.01$ very significant (**), $0.01 < p < 0.05$ significant (*), and $p \geq 0.05$ not significant (ns).

Results and discussion

Physico-chemical characterization of HHP407

The ATR-FTIR spectra of HHP407 and P407 are presented in Fig. S1 (ESI†). The appearance of the typical vibrational bands of the urethane domains in the HHP407 spectrum proved its successful synthesis. In detail, the peak at around 1720 cm^{-1} is ascribed to the stretching of the C=O domains, while the peak at 1530 cm^{-1} is attributed to the simultaneous bending and stretching of the N–H and C–N chemical regions, respectively. Moreover, the typical broad vibrational band at around 3350 cm^{-1} corresponds to the N–H stretching. The absence of a signal at *ca.* 2200 cm^{-1} suggests the complete conversion of the isocyanate groups of HDI. In addition, the characteristic vibrational bands of P407 were detected at 1250 cm^{-1} (CH$_2$ stretching), 2880 cm^{-1} (CH$_2$ rocking) and 1100 cm^{-1} (C–O–C stretching). Nonetheless, no peaks due to the end-capping molecule (*i.e.*, HEMA) were detectable, probably because they overlapped with the peaks related to the macrodiol and in-chain urethane domains. The SEC results provided $\overline{M}_n$ equal to 22 kDa and a dispersity index of 1.7. The low *Đ* value proved the synthesis of a PEU with a narrow molecular weight distribution as a result of the good control of the polymerization procedure. The ^{1}H NMR characterization of HHP407 in D$_2$O was performed to detect the presence of HEMA domains, thus proving the effectiveness of the end-capping procedure. As shown in Fig. 2, the typical peaks of HEMA were detected at 6.15, 5.85 and 1.95 ppm. Moreover, the end-capping procedure produced polymeric chains containing approximately 1.25–1.5 HEMA units per chain (*i.e.*, up to 75% end-capping yield), where the maximum theoretical value is 2 (*i.e.*, 100% end-capping yield). This result indicates a reliable end-capping reaction during the second step of PEU synthesis. The thermo-sensitive behavior of
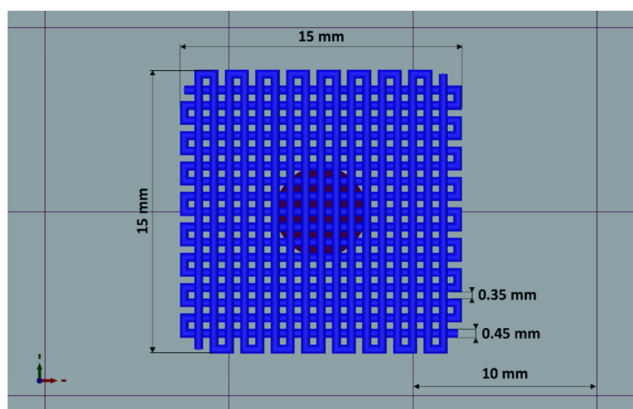

Fig. 1 Top view of the CAD model used to evaluate the 3D-extrudability of the HHP407-based hydrogel.
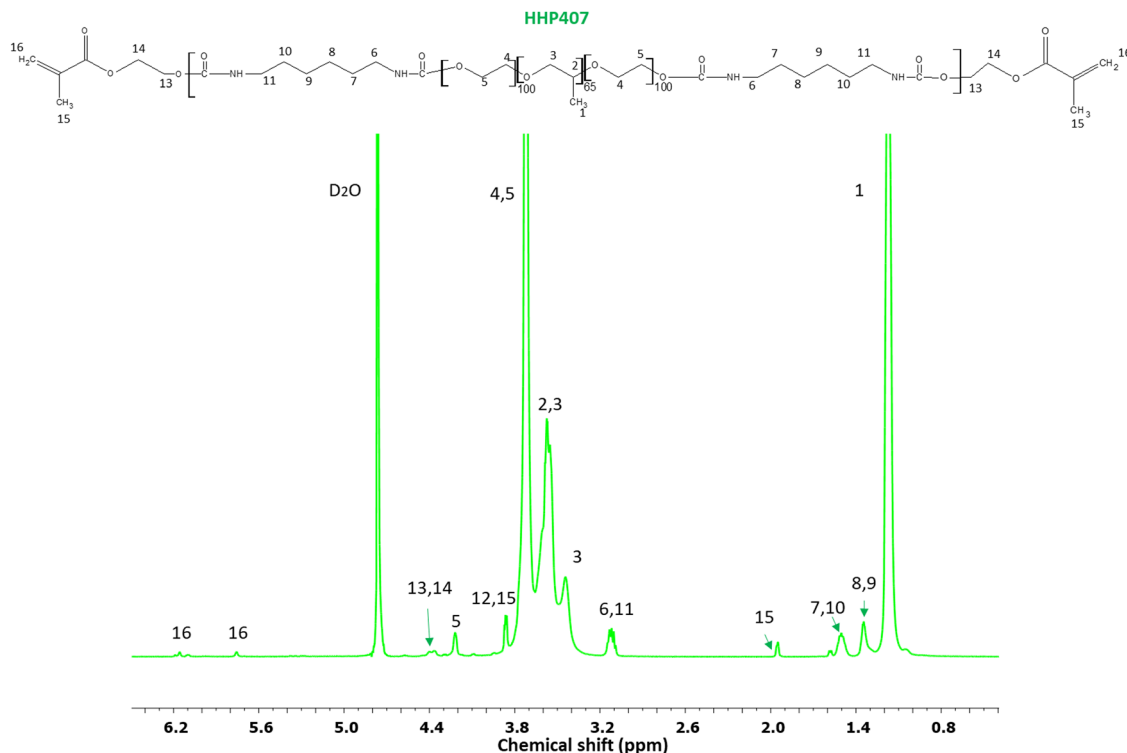
This journal is © The Royal Society of Chemistry 2024

J. Mater. Chem. B, 2024, **12**, 8389–8407 | **8395**

Fig. 2 ^{1}H NMR spectrum of HHP407. All PEU-related proton peaks are indicated by specific numbers and arrows. The presence of typical HEMA domains is indicated by protons 13 and 14 (about 4.2–4.4 ppm), 15 (1.95 ppm) and 16 (5.85 and 6.1 ppm).

HHP407-based solutions (1% w/v concentration) was evaluated in PBS and ddH$_2$O. Fig. S2 and S3 (ESI†) present the CMT curves (*i.e.*, absorbance at 356 nm *vs.* temperature) and the DLS volume patterns, respectively, for HHP407 solutions with a concentration of 1% w/v. Interestingly, HHP407 solubilized in pure water showed a CMT value of 22.2 °C, while the same formulation prepared in PBS was characterized by a CMT equal to 19.6 °C. This relevant difference can be ascribed to the salting-out effect generated by the presence of dissolved PBS ions, similar to that reported for previously studied P407-based PEUs.[21] Interestingly, HHP407 was characterized by comparable CMT values to that of chain-extended P407-based PEUs at an equal concentration (*i.e.*, 1% w/v), although its molecular mass was significantly lower (*i.e.*, around 30%).[33] The correlation between these results suggests an enhancement in the thermo-induced self-assembly of the HHP407 chains into micelles probably originated from a better balance between the overall hydrophobicity and length of the polymer chains. It is also plausible that the presence of end-methacrylate groups could induce a significant contribution in this regard. The DLS measurements showed that both analyzed samples underwent polymer chain organization into micellar structures, with some differences ascribed to the solubilization medium, and in particular the absence of dissolved ions in the sample prepared in ddH$_2$O. Indeed, at 25 °C the micelle hydrodynamic diameter was measured to be 18.5 ± 5.2 nm and 34.5 ± 3.5 nm for HHP407 solubilized in ddH$_2$O and PBS, respectively. Irrespective of the solubilization medium,

the micelle hydrodynamic diameter increased with an increase in temperature to 37 °C, reaching 41.2 ± 7.3 nm and 44.6 ± 5.8 nm for the samples prepared in ddH$_2$O and PBS, respectively (statistically significant increase for the sample prepared in ddH$_2$O, p = 0.0118). Interestingly, polymer solubilization in PBS produced significantly large micelles at 25 °C (statistically significant difference, p = 0.0115), in accordance with the lower CMT value estimated for this sample, which could initiate the micellization process at lower temperature. Conversely, when HHP407 was solubilized in ddH$_2$O, the same micelle dimensions were achieved with an increase in temperature to 37 °C (34.5 ± 3.5 nm for HHP407 1% w/v in PBS at 25 °C *vs.* 41.2 ± 7.3 nm for HHP407 1% w/v in ddH$_2$O at 37 °C, not statistically significant difference), in accordance with the higher temperature needed for this sample to initiate the polymeric chain organization into micellar structures.

Characterization of HHP407–CD SM complexes

The mixture containing HHP407 at 1% w/v and CDs at 7.6% w/v (*i.e.*, 100% theoretical PEO domain coverage, HHP407 1%–SM 100%) in ddH$_2$O resulted in a 100% recovery (calculated according to eqn (1)). This result indicates that HHP407 was a more effective polymer in terms of interaction with CDs in aqueous environments compared to previously characterized chain-extended P407-based PEUs, which were characterized by a maximum recovery of 60%.[20,21] Indeed, HHP407 was probably characterized by the best match between molecular mass and resulting hydrophobicity, which could enhance its self-assembling
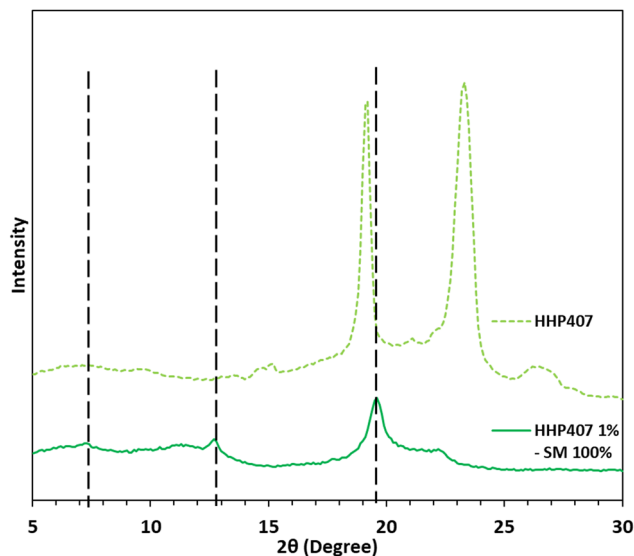
8396 | *J. Mater. Chem. B*, 2024, **12**, 8389–8407

This journal is © The Royal Society of Chemistry 2024

Fig. 3 XRD patterns of HHP407 (light green dashed line) and HHP407 1%–SM 100% (green continuous line). Typical peaks of channel-like PPR-based crystals are indicated by black vertical dashed lines at 2θ values of 7.4°, 12.8° and 19.6°. The pattern of pure HHP407 is also reported for comparative purposes.

Table 2 Gelation time at 25 °C for SM hydrogel formulations containing HHP407 at 1% and 5% w/v and CDs between 7% and 10% w/v. O.N. = overnight incubation to complete the sol-to-gel transition

		CDs (% w/v)			
		7	8	9	10
HHP407 (% w/v)	1	O.N.	4 h 20′	2 h 15′	1 h 5′
	5	O.N.	3 h	50′	20′

ability in forming micelles, and thence PPR-based networks in solution. ^{1}H NMR characterization was performed on the resolubilized HHP407 1%–SM 100% crystalline powder to clearly confirm the co-presence of HHP407 and CDs within the collected sample, as reported in Fig. S4 (ESI†). In fact, the presence of the characteristic peaks of CDs was found within the chemical shift range of 4.05 to 3.55 ppm and at 5.08 ppm, while the PEU resonance domains were detected within the chemical shift region between 1.60 and 0.95 and at 3.75 ppm. The XRD patterns demonstrated the formation of PPR-based channel-like crystalline structures within the HHP407 1%–SM 100% sample, as reported in Fig. 3. Indeed, three main peaks at 2θ values of 7.4°, 12.8° and 19.6° were detected and clearly represented the formation of SM crystals within the HHP407-based network, as notably indicated in the literature.[37] Instead, the pattern of native HHP407 powders was characterized by the presence of the same peaks that were found in chain-extended P407-based PEUs (*i.e.*, at 2θ values of 19° and 23.3°),[20,21] which were comparable to that of P407, thus suggesting that the molecular mass distribution profile and the introduced hydrophobic domains in HHP407 PEU did not influence the crystallization process of the P407 block significantly.

Design of HHP407-based SM hydrogels

Gelation properties of SM formulations based on HHP407 and CDs. The high affinity of HHP407 for interaction with CDs clearly indicated that a thorough investigation of the hydrogel formulation design could led to the definition of the best composition for the intended purposes. For this reason, a wide plethora of hydrogel formulations was produced at the maximum PEU content of 5% w/v and their gelation time was qualitatively evaluated, as reported in Table 2. Interestingly, no phase-separation phenomena were observed and all the

estimated gelation time values were significantly lower compared to that of identically formulated samples based on other PEUs developed in previous works.[20,21] For instance, the HHP407 1%–CD 10% hydrogel sample was characterized by a gelation time of around 1 h and 5 min at room temperature (*i.e.*, 25 °C), while overnight incubation was necessary for identical formulations based on previously characterized PEUs.[20,21] By decreasing CD concentration to 8% w/v, the gelation process was still characterized by extremely fast kinetics. In detail, HHP407 1%–CD 8% required only 4 h and 20 min to change into a turbid hydrogel, while 3 h were necessary for HHP407 5%–CD 8%. Thence, the properties of HHP407 in terms of balance between molecular mass and hydrophobicity (*i.e.*, poly(propylene oxide) (PPO) block dimensions and distribution along PEU chains) could be considered as highly effective to enhance the interaction with CDs.

Thus, considering all the above-mentioned reasons, among the HHP407-based hydrogel formulations, the hydrogels containing CDs at 8% w/v concentration were selected for further investigations. This selection was driven by the concurrent possibility to significantly decrease the CD content with respect to the previously developed formulations based on chain-extended PEUs (*i.e.*, CD content 20% lower),[21] while keeping the gelation relatively fast. Additionally, this novel design would provide clear advantages in terms of hydrogel production-related costs.

Biological characterization of SM hydrogels based on HHP407 and CDs. The biocompatibility of the hydrogel extracts was tested according to the ISO 10993-5 regulation. Fig. 4a and b show the Live/Dead images and quantification of the released lactate dehydrogenase and cell metabolic activity, respectively, of the HHP407 X%–CD 8% samples before and after UV irradiation (sample acronyms HHP407 X%–CD 8% and HHP407 X%–CD 8% UV, respectively). Moreover, the same formulations prepared without the addition of LAP (*i.e.*, HHP407 X%–CD 8% w/o LAP) were also tested to evaluate the effects of the photo-initiator on cell viability. Irrespective of the formulation, all the tested conditions showed a low number of dead cells (Fig. 4a), thus suggesting a high cytocompatibility of the hydrogel extracts in terms of both system composition and crosslinking process. Indeed, as further quantitatively supported (Fig. 4b), no statistically significant differences were observed in the cell viability and cytotoxicity percentages of the photo-crosslinked samples with respect to their corresponding not-irradiated formulations. Conversely, both HHP407 1%–CD 8% and HHP407 5%–CD 8% gave slightly lower cell viability values compared to the corresponding LAP-free or photo-crosslinked

This journal is © The Royal Society of Chemistry 2024

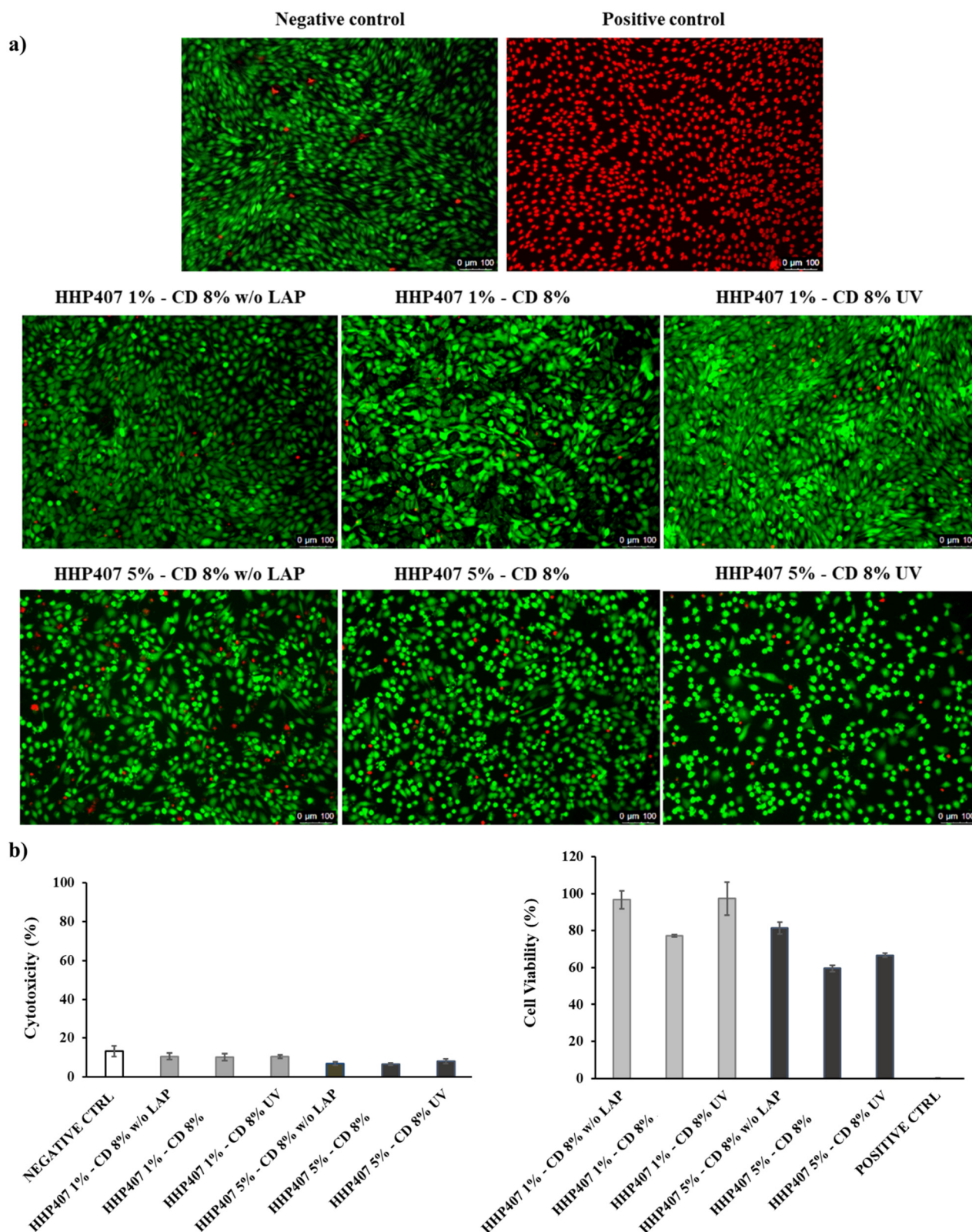*J. Mater. Chem. B*, 2024, **12**, 8389–8407 | 8397

Fig. 4 (a) Live and dead staining images of NIH-3T3 murine fibroblasts treated with HHP407 X%–CD 8%-based extracts after 24 h of incubation under normal culture conditions. Live and dead cells are stained in green and red, respectively. (b) Evaluation of NIH-3T3 cytotoxicity and cell viability induced by HHP407 X%–CD 8%-based extracts prepared according to ISO 10993-5 rules and tested through CytoTox-ONE™ and CellTiter-Blue assays, respectively.

8398 | J. Mater. Chem. B, 2024, 12, 8389–8407

This journal is © The Royal Society of Chemistry 2024

formulations. This behavior can be reasonably attributed to the release of unreacted LAP molecules in the medium, which could potentially induce intrinsic cytotoxic effects by interacting with the cells and destroying their membrane. Although the cells treated with the extracts derived from the formulations containing 5% w/v HHP407 content showed low cytotoxicity and high cell viability percentages, from a morphological point of view, cells appeared round-shaped after 24 h of culture with respect to those treated with lower HHP407 content extracts. This condition suggested a suffering cell state with reduced cell metabolic activity, as previously assessed for similar PEU hydrogels.[36] However, this evidence cannot be ascribed to the effects induced by the release of the polymeric component in the medium. Indeed, the systems with 5% w/v HHP407 content are expected to show higher stability compared to those with 1% w/v concentration, in accordance with previous works on similar formulations.[20,21] Furthermore, this behavior was even more evident upon photo-irradiation, thus further supporting this hypothesis, because photo-crosslinked systems were significantly more stable compared to the corresponding physical hydrogels (Fig. S5, ESI†). Conversely, the induction of cell quiescent conditions can be attributed to the release of high amounts of CDs. Indeed, as illustrated in Fig. S6 (ESI†), the presence of low CD concentrations (i.e., up to 6 mg mL^{-1}) in the medium did not remarkably alter the cell viability, but a further increase in CD content progressively led to increased cytotoxicity and reduced cell proliferation. Although the investigated formulations possessed the same CD content (i.e., 8% w/v), their interaction with the polymeric component was completely different. In detail, in the systems with HHP407 at a concentration of 1% w/v, CDs strongly interacted with the PEU chains, forming PPRs. Conversely, by increasing the polymeric content, the characteristic thermo-responsive behavior of the amphiphilic polymers slightly hindered complex formations in favor of micelle arrangement and aggregation. Consequently, the amount of CDs involved in the interactions with HHP407 chains was lower in HHP407 5%–CD 8% compared to HHP407 1%–CD 8%, indicating that higher CD contents were free to be released in the medium, and thus induce the slight cytotoxicity we observed. Nevertheless, both HHP407-based formulations can be considered cytocompatible

according to the ISO rules, giving cell viability percentages higher than 70% under all the tested conditions. Hence, these results, in addition to the physical characterization of the hydrogel systems, confirmed their suitability for release tests of Cur under physiological-like conditions.

Characterization of curcumin-loaded SM hydrogels based on HHP407 and CDs

Physical and mechanical characterization. HHP407 1%–CD 8% and HHP407 5%–CD 8% were selected for Cur encapsulation and release tests. In this study, a novel protocol for the production of SM hydrogels containing higher Cur payloads compared to our previous work was optimized.[21] In detail, a solution containing CDs at 14% w/v in PBS/LAP was exploited to suspend Cur at a concentration of 1 mg mL^{-1}. A homogeneous suspension of Cur was obtained with the aid of ultrasonication for 3 min under vigorous stirring and the final product is presented in Fig. S7 (ESI†). The overall stability of the resulting suspension of Cur- and CD-based complexes was restricted within a temporal range of 30 min under static condition at 25 °C; then, precipitation phenomena started to occur. Within the temporal frame of stability of the produced Cur suspension, specific aliquots were added to previously prepared HHP407-based solutions in PBS/LAP, thus producing SM hydrogels containing CDs at 8% w/v and Cur at 570 μg mL^{-1}. The resulting samples (i.e., HHP407 1%–CD 8% Cur and HHP407 5%–CD 8% Cur) were compared with the corresponding control samples not containing Cur (i.e., HHP407 1%–CD 8% and HHP407 5%–CD 8%). The effects of Cur loading on hydrogel gelation were evaluated through rheological and photo-rheological characterization. Fig. 5 displays the trends of the storage and loss moduli (G′ and G″, respectively) as a function of applied strain (i.e., strain sweep tests). Interestingly, the SM hydrogels based on HHP407 at 1% w/v concentration revealed better mechanical properties with respect to the formulations with a higher PEU content, both in the presence and in the absence of Cur. For example, G′ within the linear viscoelastic region (i.e., G′$_{LVE}$) for HHP407 1%–CD 8% was equal to 6400 Pa, while that for HHP407 5%–CD 8 was 3800 Pa (i.e., approx. 40% lower than the G′$_{LVE}$ of
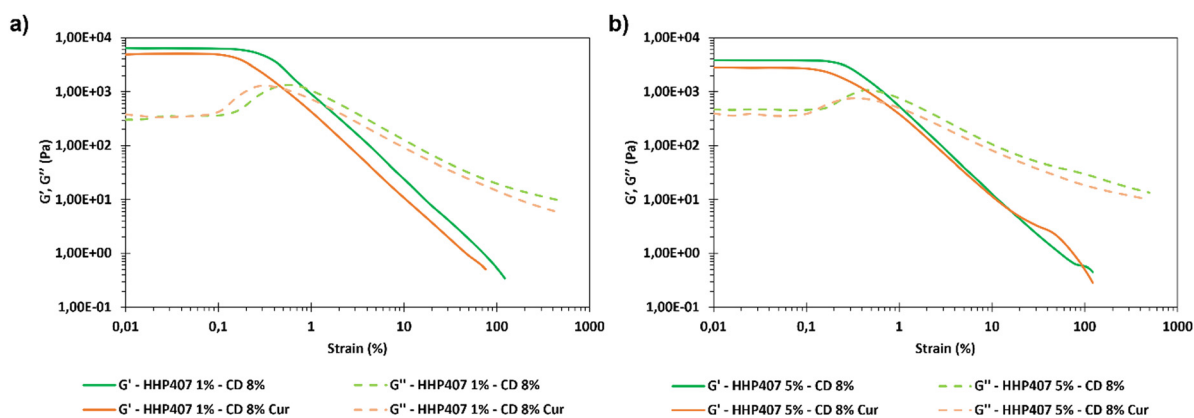
Fig. 5 G′ (continuous lines) and G″ (long dashed lines) as a function of applied strain at 37 °C for (a) HHP407 1%–CD 8% (green) and HHP407 1%–CD 8% Cur (orange), and (b) HHP407 5%–CD 8% (green) and HHP407 5%–CD 8% Cur (orange).

This journal is © The Royal Society of Chemistry 2024

J. Mater. Chem. B, 2024, **12**, 8389–8407 | **8399**

HHP407 1%–CD 8%). This interesting result can be ascribed to the lower PEU/CD mass ratio that characterized HHP407 1%–CD 8% with respect to HHP407 5%–CD 8%, as hypothesized in previous studies.[20] In this regard, it has been demonstrated that PEU solutions at low concentration (*i.e.*, 1% w/v) are generally characterized by a higher tendency to form supramolecular structures with CDs. This behavior is related to the limited occurrence of aggregate formation under this condition, while at a higher PEU content (*i.e.*, 5% w/v), the self-assembly of micellar structures significantly interferes with PPR formation. This hypothesis is in complete accordance with previous studies.[38] The presence of Cur induced a decrease in G'_{LVE} by 20% and 26% for the formulations containing HHP407 at 1% and 5% w/v, respectively. Moreover, slightly lower critical strain values (γ_L, extreme strain value of the LVE) were observed for the hydrogels containing Cur with respect to the control samples. For example, the γ_L value for HHP407 1%–CD 8% was around 0.3%, while that for the system containing Cur was measured to be around 0.1%. However, the encapsulation of a notably high Cur payload (*i.e.*, 570 µg mL^{-1}) did not induce any detrimental effect from a general perspective. Additionally, all the investigated hydrogels showed a relevant self-healing ability (Fig. S8, ESI†). Indeed, G'_{LVE} after complete rupture at 500% strain and recovery in quiescent state at 37 °C for 15 min was greater than 88% for all the investigated hydrogel systems. In this regard, the hydrogels composed of HHP407 at a concentration of 1% w/v showed a higher self-healing capacity compared to the formulations with a PEU content of 5% w/v. Indeed, the HHP407 1%–CD 8% systems exhibited recovery values of 97% for the control condition and 93% for the network containing Cur, while for hydrogel systems with a HHP407 concentration of 5% w/v, 88% recovery was calculated for both cases. These different responses can be attributed to the hindered SM crystallization due to the formation of micelle-based structures within the samples containing a higher amount of HHP407 (*i.e.*, 5% w/v), which were observed to be highly thermo-sensitive through CMT evaluation tests and DLS analyses.

Frequency sweep tests were conducted at 25 °C, 30 °C and 37 °C with the aim to evaluate the behavior of HHP407-based hydrogels in terms of network development and thermo-responsiveness. All the investigated formulations showed a fully developed gel state at each tested temperature and no cross-over points between G' and G'' were identified, as reported in Fig. S9 (ESI†). A slight dependence in the G' and G'' trends on temperature was observed for all the hydrogel systems. For example, even the formulation containing the lowest amount of thermo-sensitive PEU (*i.e.*, HHP407 1%–CD 8%) showed a G' equal to 5700 Pa at 25 °C (at 100 rad s^{-1} applied angular frequency), while that at 37 °C was 7400 Pa. Interestingly, the formulation containing HHP407 at 1% w/v showed a better developed hydrogel network compared to that containing PEU at a concentration of 5% w/v. Indeed, the former was characterized by a less marked dependency of G' and G'' on the angular frequency compared to the latter. Even the frequency sweep tests evidenced the better mechanical properties of the hydrogel composed of HHP407 at a concentration of 1% w/v with respect to that containing PEU at 5% w/v.

For example, G' at 37 °C (100 rad s^{-1}) was 7400 Pa for HHP407 1%–CD 8% and 5000 Pa for HHP407 5%–CD 8%. Cur loading induced a slight decrease in the characteristic mechanical parameters, as previously observed and discussed. The contribution of Cur was more evident in the samples containing HHP407 at 5% w/v compared to that at 1% w/v PEU concentration, probably because of the presence of a less developed SM hydrogel network at a higher PEU/CD mass ratio (*i.e.*, HHP407 at 5% w/v). However, no significant effects of Cur on hydrogel development were generally observed, given that G' and G'' of the Cur-loaded hydrogels showed consistent trends over the applied angular frequency at all the investigated temperatures with respect to the control samples. The self-healing tests evidenced a remarkable recovery ability of all the investigated HHP407-based hydrogels, as reported in Fig. 6. In fact, a G' recovery greater than 85% after 3 rupture cycles was observed for all the investigated systems. Higher recovery values were measured for the samples with an HHP407 concentration of 5% w/v (*i.e.*, around 95%) compared to those at 1% w/v (*i.e.*, around 88%). This difference can be ascribed to a better fatigue resistance of the hydrogel systems containing PEU at a higher concentration (*i.e.*, 5% w/v) due to the relatively higher damping effect originating from the more diffused and interacting amorphous domains[39] (*i.e.*, PEU chains not involved in the formation of SM crystals) with respect to the hydrogel networks with a lower PEU/CD ratio (*i.e.*, 1% w/v). Indeed, this condition generally favored the organization of the available PEU chains into stiffer PPR-based networks. Finally, the presence of Cur did not significantly affect the mechanical response of the resulting hydrogels to applied rupture cycles and recovery phases. Lastly, photo-rheological tests were performed with the aim to assess the photo-responsiveness of the developed SM hydrogels. In this regard, the typical turbidity of these systems can represent an important impediment to light transmission within the entire hydrogel volume. Nonetheless, all the gels showed good responsiveness to UV light exposure, as highlighted in Fig. 7, showing the trend of complex viscosity (η^*) as a function of time during light irradiation. Indeed, the complex viscosity (η^*) increased during light irradiation for all the tested formulations, where an η^* increase of *ca.* 16%, 8%, 17% and 12% was measured for HHP407 1%–CD 8%, HHP407 1%–CD 8% Cur, HHP407 5%–CD 8% and HHP407 5%–CD 8% Cur, respectively. A similar trend was also observed for the storage modulus, where G' increased after UV light exposure to around 19% and 17% for the HHP407 1%–CD 8% and HHP407 5%–CD 8% hydrogels, respectively.

Differently, an 8% and 11% increase in G' was observed on average for the hydrogel systems containing Cur at 570 µg mL^{-1} and PEU at 1% and 5% w/v concentration, respectively. These results suggest a lower photo-curing potential for the Cur-loaded systems due to the typical Cur photo-sensitivity, which provided a contribution in terms of UV light dissipation. Interestingly, the visual inspection of the sample containing HHP407 at 1% w/v and Cur indicated a significant reduction in its original intense orange color. This observation indicated the indisputable degradation of a relevant amount of Cur payload
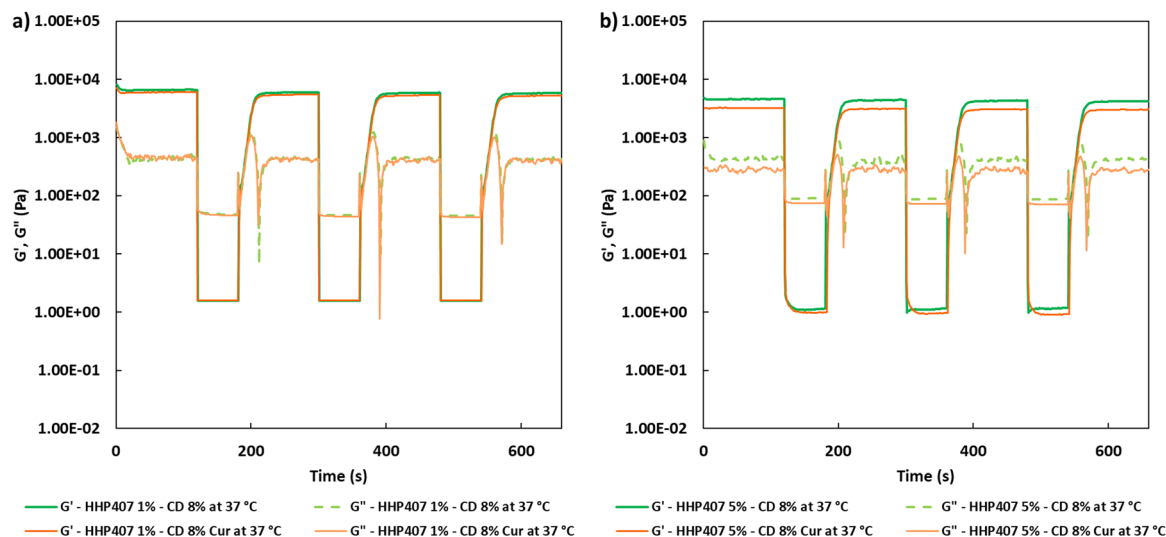
8400 | *J. Mater. Chem. B*, 2024, **12**, 8389–8407

This journal is © The Royal Society of Chemistry 2024

Fig. 6 Strain test curves showing G' (continuous lines) and G'' (dashed lines) as a function of time during cyclic rupture (100% strain, 60 s) and recovery (0.1% strain, 120 s) of hydrogel networks at (a) 1% and (b) 5% w/v HHP407 concentration at 37 °C. Control hydrogels (green lines) are compared to the hydrogels containing Cur at 570 µg mL^{-1} (orange lines).
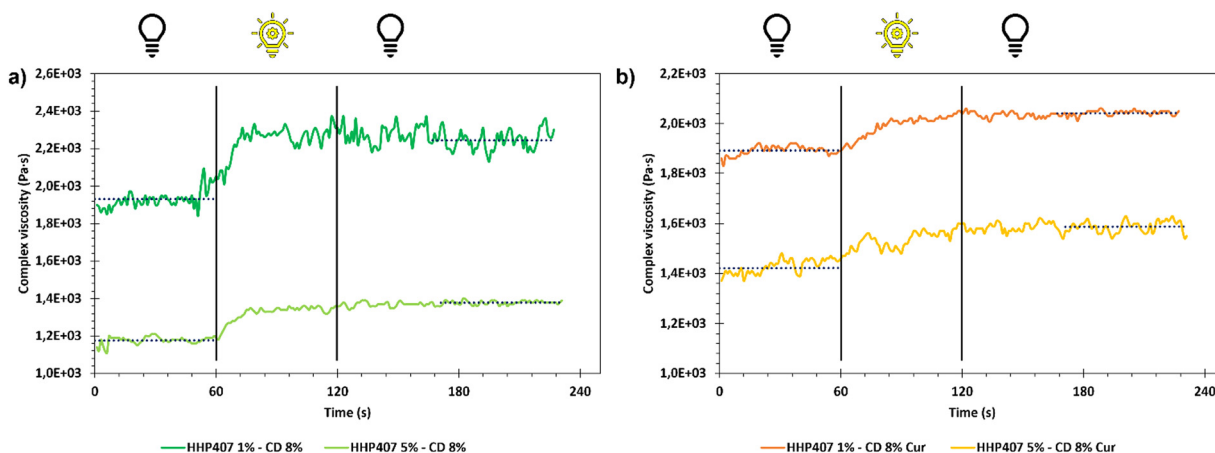

Fig. 7 Complex viscosity as a function of time for hydrogels (a) at 1% and 5% w/v HHP407 concentration and (b) containing Cur at 570 µg mL^{-1}. Hydrogels were characterized before photo-crosslinking for 60 s. Then, exposure to UV light (365 nm, 10 mW cm^{-2}) was conducted for 60 s and the resulting mechanical properties were registered for additional 120 s. Horizontal dotted blue lines identify the mean complex viscosity values before (in the first 60 s of observation) and after photo-curing (in the last 60 s of observation).

within the hydrogel network containing PEU at a low concentration. Differently, no significant color changes were observed for the HHP407 5%–CD 8% samples, thus suggesting that a higher content of photo-sensitive PEU helped to preserve the Cur payload. This behavior can be ascribed to two main aspects. Firstly, a significantly higher number of photo-sensitive groups was intrinsically present in the formulation containing HHP407 at 5% w/v compared to 1% w/v, thus competing with the Cur degradation process in terms of UV light absorbance through the formation of chemical crosslinks. Secondly, it is likely that a higher content of PEU is beneficial in terms of the stabilization and protection of Cur from degradation through its encapsulation in more available hydrophobic domains. In conclusion, the performed photo-rheological

characterization suggested that a shorter UV light exposure was sufficient to achieve complete crosslinking and this aspect was particularly relevant for the samples containing HHP407 at a low concentration (*i.e.*, 1% w/v). Specifically, the results suggested that almost complete crosslinking was achieved within 20–30 s of UV light irradiation for all the investigated hydrogels, as can be observed in the complex viscosity curves reported in Fig. 7.

Release profiles of Cur encapsulated within HHP407-based hydrogels. Release studies were performed on Cur-loaded SM hydrogels subjected to only physical crosslinking (acronym HHP407 X%–CD 8% Cur) or the double crosslinking process (*i.e.*, physical + chemical crosslinking) (acronym HHP407 X%–CD 8% Cur UV). The quantification of the released drug
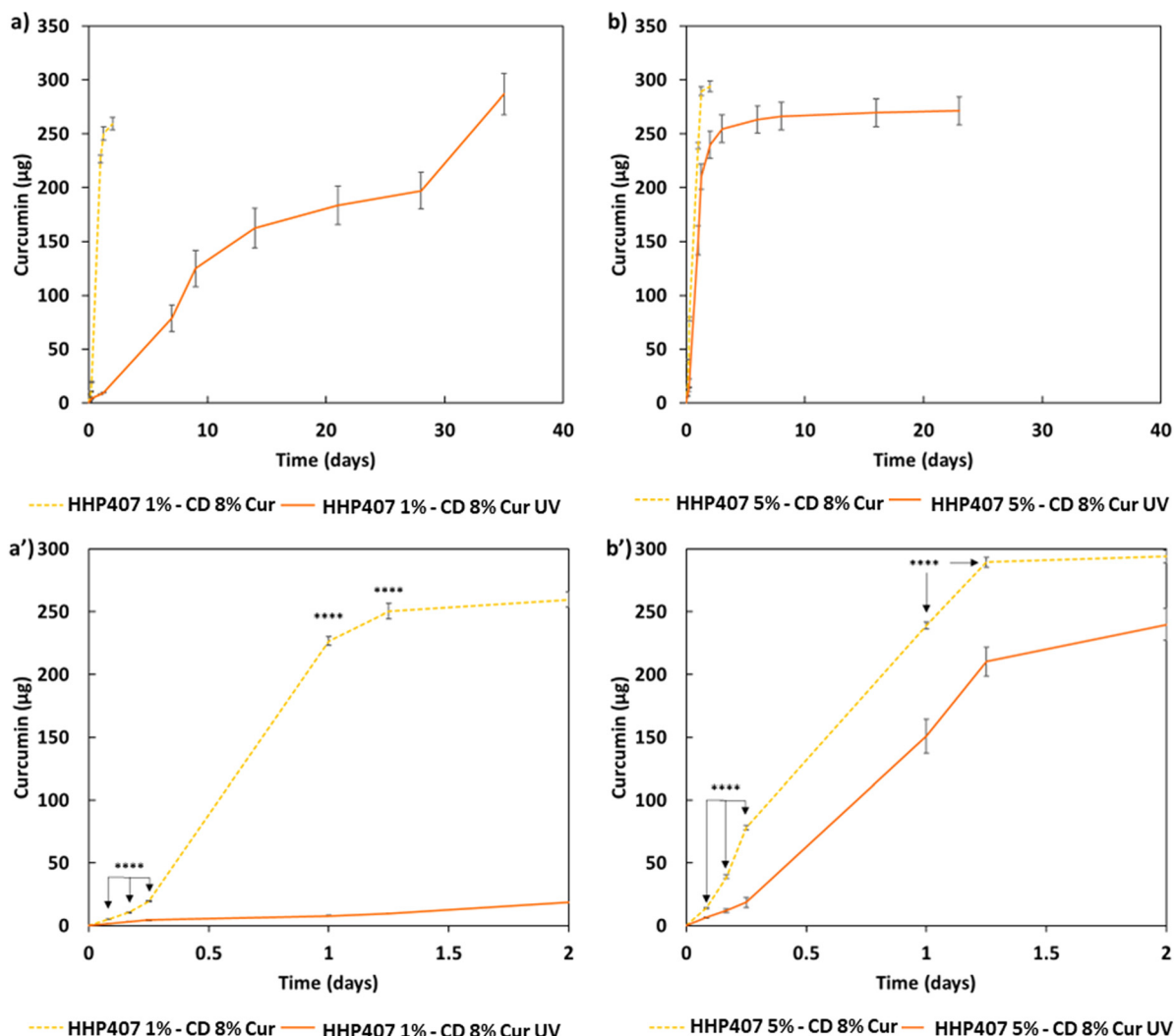
Fig. 8 Cur release profiles from hydrogel systems in contact with PBS at 37 °C and characterized by different HHP407 contents: (**a**) and (**a′**) 1% w/v (HHP407 1%–CD 8% Cur and HHP407 1%–CD 8% Cur UV) and (**b**) and (**b′**) 5% w/v (HHP407 5%–CD 8% Cur and HHP407 5%–CD 8% Cur UV). Physical hydrogels (light orange dashed lines) are compared with photo-cured systems (orange continuous lines). (a′) and (b′) graphs represent the release profile in detail measured within the first 2 days of observation.

was conducted using specific calibration curves based on standard samples prepared from a stock solution obtained by re-solubilizing the hydrogel systems in PBS. This procedure was necessary in this case because the high amount of encapsulated Cur (*i.e.*, 570 μg mL^{-1}) induced a highly more important contribution to the involved PEU in terms of solubilization and delivery of the drug with respect to our previous study, where the PEU content ranged within 1% and 3% w/v and Cur was loaded at 80 μg mL^{-1}.[21] In this study, the involvement of specific PEU-dependent structures was hypothesized, as suggested from the available literature on the design of Cur-loaded systems based on amphiphilic polymers.[40,41] The calibration curves obtained from the HHP407 1%–CD 8% and HHP407 5%–CD 8% samples are reported in Fig. S10 (ESI†). Totally different calibration curves were obtained, although the only difference between these samples was related to the PEU content. In detail, a higher molar extinction coefficient was

estimated for the system containing HHP407 at 5% w/v with respect to that at 1% w/v PEU concentration, indicating an enhanced integration and solubilization of Cur at a higher PEU concentration. Moreover, notably good linear fittings were calculated.

The release profiles of Cur from all the hydrogels (*i.e.*, HHP407 1%–CD 8% Cur, HHP407 1%–CD 8% Cur UV, HHP407 5%–CD 8% Cur, HHP407 5%–CD 8% Cur UV) showed significantly different trends, which were correlated with the hydrogel formulation and crosslinking method, as shown in Fig. 8. Generally, the systems exposed to UV light showed a delayed delivery of Cur and could sustain this process for up to 35 days of incubation under physiological-like conditions (*i.e.*, in contact with PBS at 37 °C). Surprisingly, the entire payload of Cur (*i.e.*, 285 μg per sample) was also released from the UV-cured systems, thus indicating the optimal preservation of its chemical stability within the SM networks, which indeed acted as protective

8402 | *J. Mater. Chem. B*, 2024, **12**, 8389–8407

This journal is © The Royal Society of Chemistry 2024

Table 3 Selected parameters for the printing process

D_E	P_E	ν_P	T_s	T_B
250 µm	35–40 kPa	10 mm s^{-1}	37 °C	37 °C

element for this highly sensitive drug. Interestingly, the SM hydrogels based on HHP407 at a concentration of 1% w/v exhibited slower release kinetics compared to those containing PEU at a concentration of 5% w/v. In particular, at each time point, a significantly higher release rate was observed for HHP407 5%–CD 8% Cur UV with respect to HHP407 1%–CD 8% Cur UV (data not shown, $p < 0.0012$). This observation can be correlated with the previous rheological and photo-rheological characterizations, in which the hydrogels composed of HHP407 at a concentration of 1% w/v showed the highest G' values, thus indicating the formation of highly rigid networks, due to the enhanced SM self-assembly into PPR-based crystals.[42,43]

Even in this case, the PEU/CD ratio suggested the formation of differently organized networks that could also undergo photo-induced crosslinking and open a way towards the possibility of finely tuning the resulting release kinetics.

Preliminary studies on HHP407-based SM hydrogel extrudability and printing

In this study, a preliminary evaluation of the general extrudability of the HHP407-based hydrogel systems was conducted. The HHP407 5%–CD 8% formulation was selected for this purpose due to its lower rigidity and generally higher

damping/self-healing ability, which were observed through rheological characterizations. These parameters are fundamental aspects to consider for the selection of a potential bio-ink or biomaterial ink.[44] The printing process was conducted by controlling different parameters including the tip extrusion diameter (D_E), extrusion pressure (P_E), printhead velocity (ν_P), syringe temperature (T_s), and bed temperature (T_B). The printing process was conducted at 37 °C for both the syringe and bed to favor the stabilization of the hydrogel network through the major contribution of hydrophobic interactions. A preliminary set of optimized parameters was obtained and reported in Table 3.

Fig. 9 shows the produced 3D-printed constructs and a qualitative comparison between the resulting geometry and the theoretical CAD design. The printing process produced constructs with good definition and acceptable printing fidelity. In fact, the filament diameter was determined to be 0.46 ± 0.08 mm (average of 5 measurements obtained from 4 different filaments), while the theoretical value was 0.45 mm, thus proving both extrudability and filament formation. The selection of a smaller tip diameter (0.25 mm) with respect to the theoretical value (0.45 mm) was driven by the need to reach the best compromise between printing velocity and required extrusion pressure. Indeed, under the selected conditions, the production of two-layer grids with a 0/90° pattern required an overall printing time of around 1 min. The pore dimensions were larger than the theoretical design, where the pore area of the printed constructs was calculated to be 0.17 ± 0.04 mm^2, which is around 40% higher than the theoretical value. This difference can be ascribed to the presence of defects in
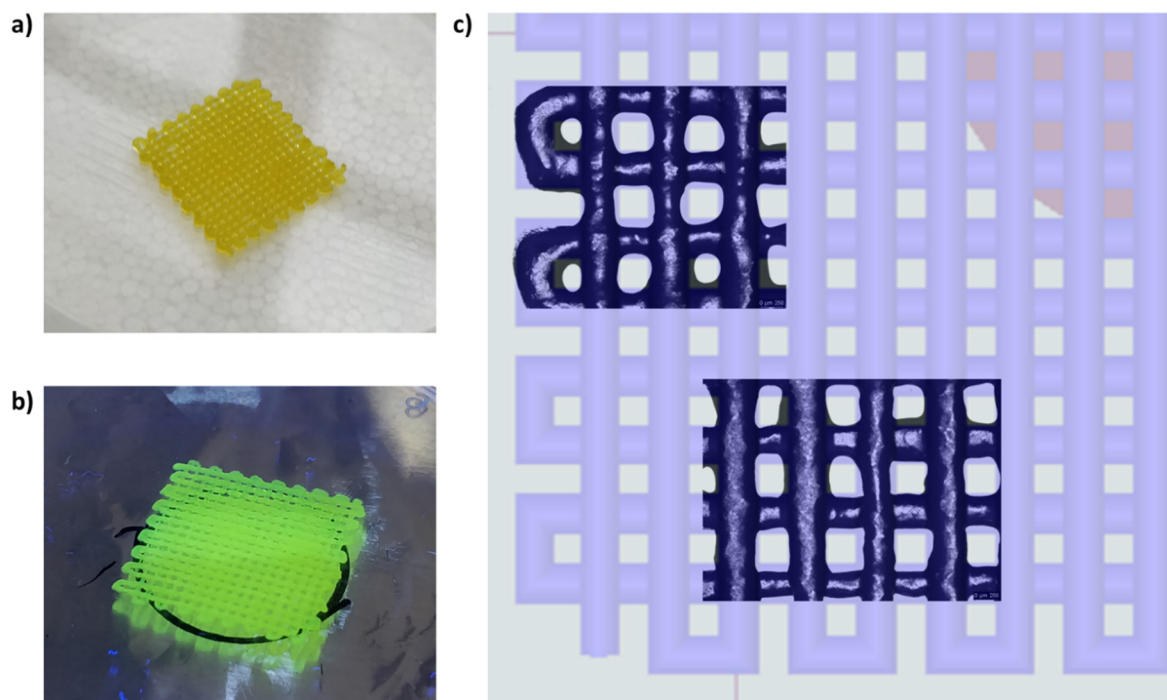

Fig. 9 (a) Photo of a 3D-printed construct based on HHP407 5%–CD 8% Cur. (b) UV curing of HHP407 5%–CD 8% Cur structures. (c) Qualitative geometrical match between the 3D-printed HHP407 5%–CD 8% Cur and the starting theoretical CAD design.
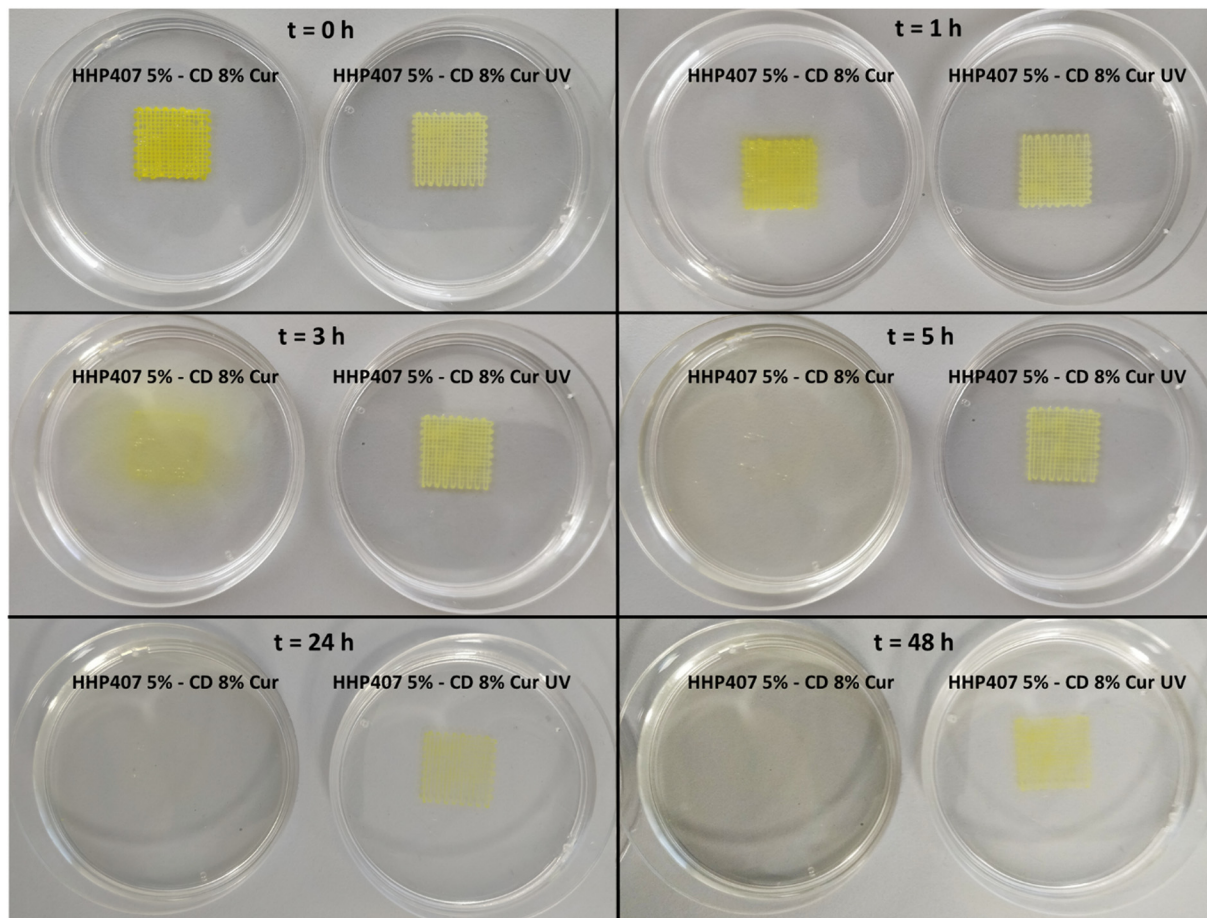
This journal is © The Royal Society of Chemistry 2024

J. Mater. Chem. B, 2024, **12**, 8389–8407 | 8403

Fig. 10 Qualitative evaluation of the stability of the 3D-printed HHP407 5%–CD 8% Cur and HHP407 5%–CD 8% Cur UV structures in contact with 5 mL of PBS at 25 °C (within a Petri support − 50 mm diameter).

proximity to the intersections between the two layers. Nonetheless, good printability could be deduced from these preliminary results. Further optimization can be done based on geometry investigation through more precise methodologies (*e.g.*, computed tomography or optical coherence tomography) to better find the correlation between morphological features and printing parameters. Another qualitative characterization was conducted in terms of stability in contact with a large volume of aqueous medium (PBS, 5 mL, 25 °C) (Fig. 10). The UV cured systems (HHP407 5%–CD 8% Cur UV) showed a significantly improved residence time in aqueous medium with respect to the physically-crosslinked sample (HHP407 5%–CD 8% Cur). In fact, as shown in Fig. 10, the UV light-irradiated samples preserved their geometrical integrity for up to 3 days of observation in a highly destabilizing aqueous environment, while physically-crosslinked samples were completely solubilized within an incubation time of 3 h.

Moreover, an evident color change was observed after UV curing for 1 min, thus indicating that the resulting relevant interfacial surface and the limited thickness of the construct probably enhanced the exposure of Cur to photo-degradation. Nonetheless, an evident yellowish color was maintained, indicating the protective effect of HHP407 and CDs on Cur even

under these particularly degradative conditions. Indeed, when the same UV curing protocol was applied to the samples utilized for Cur release studies, it did not induce any evident Cur degradation phenomena due to the concurrent protective effect provided by HHP407/CDs and the selected sample geometry (*i.e.*, thickness and overall volume). Lastly, the HHP407 5%–CD 8% hydrogel formulation was successfully used to print 25-layer (300 μm layer thickness) cylinder constructs with a 0/90° pattern. The layer-by-layer photo-curing process effectively stabilized each 3D printed layer, resulting in a self-standing construct with a final height of *ca.* 0.75 mm, which is in agreement with the expected theoretical value. Fig. 11 presents the macroscopic appearance of the 3D printed structures during fabrication (Fig. 11a) and at the end of the printing process, highlighting the absence of evident structure collapse and consequent pore closing phenomena (Fig. 11b).

Conclusions

In this work, a novel photosensitive PEU was synthesized by modifying a well-known and optimized synthesis process.[21,23,25] Indeed, HHP407 PEU was synthesized using HEMA as the
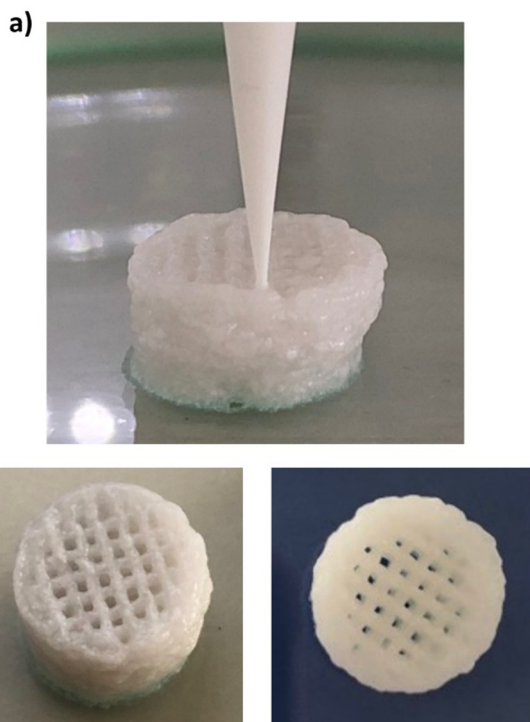
8404 | *J. Mater. Chem. B*, 2024, **12**, 8389–8407

This journal is © The Royal Society of Chemistry 2024

Fig. 11 (a) Photograph of HHP407 5%–CD 8%-based 25-layer cylinder construct with a 0/90° pattern taken during the 3D printing process and (b) macroscopic appearance of 3D printed 25-layer cylinder constructs with a 0/90° pattern at the end of the printing process.

end-capping alcohol of the isocyanate-terminated prepolymer chains resulting from the prepolymerization reaction between P407 and HDI.

The performed physico-chemical characterization indicated a good functionalization of the resulting PEU chains through the exposure of methacrylate end-groups. Moreover, excellent thermo-sensitivity was assessed by CMT evaluation and DLS analyses, although HHP407 possessed a lower molecular mass compared to the chain-extended 407-based PEUs previously developed by our group.[21] This behavior suggested the achievement of a well-balanced polymer structure and hydrophobicity in terms of length and distribution of the available domains (i.e., PPO, HDI and probably also HEMA). Because of the resulting physico-chemical properties, HHP407 was demonstrated to be suitable for the formation of PPR-based crystals in an aqueous environment. Moreover, it was found to be a particularly suitable polymer for the formation of SM networks among the plethora of materials investigated in the literature.[21,43] Hence, it is likely that its structural features represent an optimized set of properties for constructive interaction with CDs, resulting in highly stable and simultaneously responsive networks. This particular behavior allowed the design of SM hydrogels with good mechanical properties at a low HHP407 content (i.e., ≤5% w/v) and a relatively low CD concentration (i.e., 8% w/v). In this regard, the formulation showing the lowest PEU/CD mass ratio (i.e., 1% and 8% w/v HHP407 and CD concentration, respectively) was characterized

by better mechanical properties with respect to the system containing HHP407 at 5% w/v, as assessed through rheological characterizations. This observation was in agreement with previous results obtained for similar systems, thus further reinforcing the hypothesis of the high functionality and tunability of PEU macromolecules at low concentrations in combination with CDs.[20,21] Although HHP407 produced highly crystalline hydrogel networks with CDs, with the consequent possibility of obtaining brittle hydrogels, obvious self-healing ability was observed. Photosensitivity was assessed by means of photo-rheological characterizations. Irrespective of the HHP407 and CD content, all the tested formulations (i.e., purely physical hydrogels and both physically and chemically crosslinked hydrogels) showed high cytocompatibility according to the ISO 10993-5 regulation. The Cur delivery studies evidenced that the hydrogel composition and consecutive photo-crosslinking play a key role in tuning the Cur release kinetics from the HHP407-based networks. Furthermore, the in vitro Cur release tests demonstrated the protective ability of HHP407 and CDs on this photo-sensitive drug, opening the way for the possibility to sustain the release of Cur in aqueous environments for up to 5 weeks. Interestingly, these samples did not show any color change upon light irradiation, resulting in the possibility to completely release the encapsulated Cur payload. Conversely, under different experimental set-ups (i.e., lower sample thickness and higher exposed surface area), we observed a slight color change in the samples (higher for samples with lower PEU content, and thus lower polymer-induced Cur protection), suggesting the occurrence of Cur photo-induced degradation. Overall, our data suggest that depending on the geometrical features of the developed construct (e.g., 3D bio-printed structure or injected deposit filling a cavity), a fine optimization of the polymerization process should be performed (e.g., by minimizing the irradiation time) to protect the loaded Cur molecules from photo-induced degradation. Finally, one formulation among the developed hydrogels was preliminary evaluated for the production of 3D-printed structures with good resolution. These results further indicated that HHP407 is a highly versatile polymer for the development of engineered devices in regenerative medicine. Hence, this study confirmed the great potential of appropriately synthesized PEUs as raw materials for the design of SM hydrogels with a low synthetic polymer content and showing good mechanical performances, progressive release profiles of encapsulated drugs, and easy processability through extrusion-based 3D bioprinting. The observed properties present insights into the future use of the herein-described hydrogel platform for 3D cell culture,[45] inject-based bioprinting[46] and vat-polymerization 3D bioprinting,[47] among others. Overall, we can conclude that the developed hydrogels can find widespread application in the emerging field of regenerative pharmacology, as (i) easily injectable drug-loaded systems suitable for the perfect filling of body defects through a mini-invasive procedure, and (ii) drug-loaded biomaterial inks in the fabrication of patient-personalized patches. Hence, the designed hydrogels hold great promise, warranting their further development and

This journal is © The Royal Society of Chemistry 2024

J. Mater. Chem. B, 2024, 12, 8389–8407 | 8405

characterization in future investigations targeting specific applications in the biomedical field (*e.g.*, wound healing, endodontics, and cartilage repair).

Author contributions

Alessandro Torchio: conceptualization, methodology, validation, formal analysis, investigation, data curation, writing – original draft, visualization. Monica Boffito: supervision, resources, conceptualization, methodology, validation, investigation, writing – review & editing, funding acquisition, visualization. Rossella Laurano: methodology, investigation, data curation, writing – original draft. Claudio Cassino: investigation, data curation, writing – review & editing. Mario Lavella: investigation, data curation, writing – review & editing. Gianluca Ciardelli: supervision, resources, writing – review & editing, funding acquisition.

Data availability

All relevant data are within the manuscript and ESI.† The data are available from the corresponding author on reasonable request.

Conflicts of interest

The authors declare that they have no known competing financial interests or personal relationships that could have appeared to influence the work reported in this paper.

Acknowledgements

References

1 R. Eelkema and A. Pich, *Adv. Mater.*, 2020, **32**, 1906012.
2 W. Hu, Z. Wang, Y. Xiao, S. Zhang and J. Wang, *Biomater. Sci.*, 2019, **7**, 843–855.
3 B. Tian, S. Hua, Y. Tian and J. Liu, *J. Mater. Chem. B*, 2020, **8**, 10050–10064.
4 Y. S. Zhang and A. Khademhosseini, *Science*, 2017, **356**, eaaf3627.

5 J. Li, Z. Suo and J. J. Vlassak, *J. Mater. Chem. B*, 2014, **2**, 6708–6713.
6 S. P. Zhao, L. M. Zhang, D. Ma, C. Yang and L. Yan, *J. Phys. Chem. B*, 2006, **110**, 16503–16507.
7 A. Harada and M. Kamachi, *Macromolecules*, 1990, **23**, 2821–2823.
8 J. Li, A. Harada and M. Kamachi, *Polym. J.*, 1994, **26**, 1019–1026.
9 X. Li and J. Li, *J. Biomed. Mater. Res. A*, 2008, **86**, 1055–1061.
10 E. Larrañeta and J. R. Isasi, *Langmuir*, 2012, **28**, 12457–12462.
11 J. Li, X. Ni, Z. Zhou and K. W. Leong, *J. Am. Chem. Soc.*, 2003, **125**, 1788–1795.
12 X. Ni, A. Cheng and J. Li, *J. Biomed. Mater. Res. A*, 2009, **88**, 1031–1036.
13 S. P. Zhao and W. L. Xu, *J. Polym. Res.*, 2010, **17**, 503–510.
14 H. Wei, A. Y. Zhang, L. Qian, H. Yu, D. Hou, R. Qiu and Z. G. Feng, *J. Polym. Sci. A Polym. Chem.*, 2005, **43**, 2941–2949.
15 H. Wei, H. Yu, A. Zhang, L. Sun, D. Hou and Z. Feng, *Macromolecules*, 2005, **38**, 8833–8839.
16 H. Wei, J. He, L. Sun, K. Zhu and Z. Feng, *Eur. Polym. J.*, 2005, **41**, 948–957.
17 D. Chimene, R. Kaunas and A. K. Gaharwar, *Adv. Mater.*, 2020, **32**, 1902026.
18 L. Xiaorui, Z. Fuyin, W. Xudong, G. Xuezheng, Z. Shudong, L. Hui, D. Dandan, L. Yubing, W. Lizhen and F. Yubo, *Int. J. Bioprint.*, 2022, **9**, 649.
19 S. Boularaoui, G. Al Hussein, K. A. Khan, N. Christoforou and C. Stefanini, *Bioprinting*, 2020, **20**, e00093.
20 A. Torchio, M. Boffito, A. Gallina, M. Lavella, C. Cassino and G. Ciardelli, *J. Mater. Chem. B*, 2020, **8**, 7696–7712.
21 A. Torchio, C. Cassino, M. Lavella, A. Gallina, A. Stefani, M. Boffito and G. Ciardelli, *Mater. Sci. Eng., C*, 2021, **127**, 112194.
22 M. Boffito, F. Di Meglio, P. Mozetic, S. M. Giannitelli, I. Carmagnola, C. Castaldo, D. Nurzynska, A. M. Sacco, R. Miraglia, S. Montagnani, N. Vitale, M. Brancaccio, G. Tarone, F. Basoli, A. Rainer, M. Trombetta, G. Ciardelli and V. Chiono, *PLoS One*, 2018, **13**, e0199896.
23 M. Boffito, E. Gioffredi, V. Chiono, S. Calzone, E. Ranzato, S. Martinotti and G. Ciardelli, *Polym. Int.*, 2016, **65**, 756–769.
24 M. Boffito, A. Torchio, C. Tonda-Turo, R. Laurano, M. Gisbert-Garzarán, J. C. Berkmann, C. Cassino, M. Manzano, G. N. Duda, M. Vallet-Regí, K. Schmidt-Bleek and G. Ciardelli, *Front. Bioeng. Biotechnol.*, 2020, **8**, 384.
25 C. Pontremoli, M. Boffito, S. Fiorilli, R. Laurano, A. Torchio, A. Bari, C. Tonda-Turo, G. Ciardelli and C. Vitale-Brovarone, *Chem. Eng. J.*, 2018, **340**, 103–113.
26 M. Ding, J. Li, H. Tan and Q. Fu, *Soft Matter*, 2012, **8**, 5414.
27 J. Hu and L. Tan, in Polyurethane composites and nano-composites for biomedical applications, *Polyurethane Polymers*, Elsevier, 2017, pp. 477–498.
28 R. Laurano, M. Boffito, M. Abrami, M. Grassi, A. Zoso, V. Chiono and G. Ciardelli, *Bioact. Mater.*, 2021, **6**, 3013–3024.
29 H. H. Tønnesen, M. Másson and T. Loftsson, *Int. J. Pharm.*, 2002, **244**, 127–135.

8406 | *J. Mater. Chem. B*, 2024, **12**, 8389–8407

This journal is © The Royal Society of Chemistry 2024

30 H. H. Tønnesen and J. Karlsen, *Z. Lebensm.-Unters. Forsch.*, 1985, **180**, 402–404.

31 Y. Nimiya, W. Wang, Z. Du, E. Sukamtoh, J. Zhu, E. Decker and G. Zhang, *Mol. Nutr. Food Res.*, 2016, **60**, 487–494.

32 M. Kharat, Z. Du, G. Zhang and D. J. McClements, *J. Agric. Food Chem.*, 2017, **65**, 1525–1532.

33 M. Wright, K. Kurumada and B. Robinson, in Rates of incorporation of small molecules into pluronic micelles, *Trends in Colloid and Interface Science XVI*, ed. Miguel, M., Burrows, H. D., Springer Berlin Heidelberg, Berlin, Heidelberg, 2004, pp. 8–11.

34 X. J. Loh, L. W. I. Cheng and J. Li, *Macromol. Symp.*, 2010, **296**, 161–169.

35 L. Wu, L. Yu, X. Fu and Z. Li, *Chin. J. Polym. Sci.*, 2015, **33**, 1140–1149.

36 R. Laurano, V. Chiono, C. Ceresa, L. Fracchia, A. Zoso, G. Ciardelli and M. Boffito, *Eng. Reg.*, 2021, **2**, 263–278.

37 J. W. Chung, T. J. Kang and S. Y. Kwak, *Macromolecules*, 2007, **40**, 4225–4234.

38 C. Pradal, K. S. Jack, L. Grøndahl and J. J. Cooper-White, *Biomacromolecules*, 2013, **14**, 3780–3792.

39 K. J. Henderson, T. C. Zhou, K. J. Otim and K. R. Shull, *Macromolecules*, 2010, **43**, 6193–6201.

40 V. Kant, A. Gopal, D. Kumar, N. N. Pathak, M. Ram, B. L. Jangir, S. K. Tandan and D. Kumar, *J. Surg. Res.*, 2015, **193**, 978–988.

41 S. Khan, M. U. Minhas, M. Ahmad and M. Sohail, *J. Biomater. Sci., Polym. Ed.*, 2018, **29**, 1–34.

42 R. S. Stowers, S. C. Allen and L. J. Suggs, *Proc. Natl. Acad. Sci. U. S. A.*, 2015, **112**, 1953–1958.

43 A. Domiński, T. Konieczny and P. Kurcok, *Materials*, 2019, **13**, 133.

44 A. Schwab, R. Levato, M. D'Este, S. Piluso, D. Eglin and J. Malda, *Chem. Rev.*, 2020, **120**, 11028–11055.

45 H. Cao, L. Duan, Y. Zhang, J. Cao and K. Zhang, *Signal Transduction Targeted Ther.*, 2021, **6**, 426.

46 W. L. Ng and V. Shkolnikov, *Int. J. Bioprint.*, 2024, 2135.

47 W. L. Ng, J. M. Lee, M. Zhou, Y. W. Chen, K. A. Lee, W. Y. Yeong and Y. F. Shen, *Biofabrication*, 2020, **12**, 022001.

This journal is © The Royal Society of Chemistry 2024

J. Mater. Chem. B, 2024, **12**, 8389–8407 | **8407**